8-1-2014

Thermal and Structural Modeling of Electrochromics on Glass

Mahesh B. Manandhar
University of Denver

THERMAL AND STRUCTURAL MODELING OF ELECTROCHROMICS ON GLASS

_____

A Thesis

Presented to

The Faculty of the Daniel Felix Ritchie School of Engineering and Computer Science

University of Denver

_____

In Partial Fulfillment

of the Requirements for the Degree

Master of Science

_____

by

Mahesh B. Manandhar

August 2014

Advisor: Dr. Mohammad Matin

Author: Mahesh B. Manandhar
Title: THERMAL AND STRUCTURAL MODELING OF ELECTROCHROMICS ON GLASS
Advisor: Dr. Mohammad Matin
Degree Date: August 2014

Abstract

Advanced glazing is a type of window glazing that interacts with the surrounding environment to change its thermal and optical properties to create a more comfortable and energy efficient indoor environment. Electrochromics are one type of such advanced glazing materials that change their properties in response to an externally applied voltage controllable by the user or by automation.

The effectiveness of electrochromics depends upon how well it can keep off extreme temperature conditions from outdoors all year round as well as how structurally stable it can remain at such conditions. This research investigates the use of COMSOL, a finite element multiphysics simulation software, to analyze the thermal and structural stability of electrochromic materials. This research successfully verifies that EC material does contribute to the reduction of thermal stress on glass surfaces as well as improve the insulation of the indoors while enhancing the thermal and structural stability of the glass.

Acknowledgements

I would like to acknowledge my deepest gratitude to my academic advisor, Dr. Mohammad Matin, for his constant guidance and supervision throughout the entirety of my research period. His mentorship and encouragement has been vital in my pursuit of this research.

I am highly obliged to my colleague Dave Alie for helping me understand the principles of electrochromics. His input and suggestions have been vital in my development of an accurate model in COMSOL.

I would like to thank my graduate committee, Dr. David Gao and Dr. Stephen Sewalk for their guidance and expertise throughout the thesis procedures. I must express my gratitude to Tim Sheu, our IT director, and the entire COMSOL support team for being patient with me and helping me with all my queries in COMSOL.

Lastly, I would like to thank my family and friends for all their encouragement and support.

Contents

List of Figures

List of Acronyms

$2\ H_2O.WO_3$	Dihydrous Tungsten Oxide
3D	Three Dimensional
a-WO_3	Amorphous Tungsten Oxide
CAD	Computer Aided Design
CE	Counter Electrochromic
C_p	Heat capacity at constant pressure
DC	Direct Current
E	Young's Modulus
EC	Electrochromic
EIA	Energy Information Administration
$Fe[Fe(CN)_6]$	Ferric Ferrocyanide
FEA	Finite Element Analysis
FEM	Finite Element Method
GUI	Graphical User Interface
H	Hydrogen
$H_2O.WO_3$	Monohydrous Tungsten Oxide
IR	Infra Red
Ir	Iridium
ITO	Tin doped Indium Oxide
k	Thermal conductivity
Li	Lithium

MEMS	Microelectromechanical System
Mo	Molybdenum
MPa	Mega Pascal
mph	Miles per hour
Na	Sodium
Nb	Niobium
Ni	Nickel
PDLC	Polymer Dispersed Liquid Crystal
PEDOT	Polyethylenedioxythiophene
POM	Polyoxometalate
PVB	Polyvinyl Butyral
RF	Radio Frequency
S1	von Mises Stress of Surface 1
S4	von Mises Stress of Surface 4
T_i	Indoor Temperature
T_o	Outdoor Temperature
T1	Temperature of Surface 1
T4	Temperature of Surface 4
TCO	Transparent Conducting Oxide
Ti	Titanium
TO	Tin Oxide
V	Vanadium
W	Tungsten

WO_3	Tungsten Oxide
α	Coefficient of thermal expansion
ρ	Density
υ	Poisson's ratio

Chapter One: Introduction

1.1 Background

The U.S. Energy Information Administration (EIA) estimated that in 2012, the commercial and residential building sector accounted for nearly 40% of the total U.S. primary energy consumption [**1**]. Space heating and cooling comprised of 48% of total consumption in homes while commercial buildings had 44% of their total consumption for the same [**1**]. This data suggests that nearly half of all energy consumed in buildings in the U.S. is for heating and cooling purposes.

Another study on energy transmission by building envelope components concludes that of the different components of building envelopes like windows, roofs, openings and floors, windows accounts for about 50% of thermal energy transmission [**2**]. With glass being used by architects and building designers for aesthetics and occupant comfort for building envelopes, these data need to be seriously considered in the optimization of the utility cost of heating and cooling of buildings. Interactive glass that can modify its thermal and optical properties according to different environmental weather conditions like solar radiation and temperatures can significantly affect this cost of heating and cooling requirements.

Such interactive glass, known in the glass industry as Advanced Glazing, can significantly reduce the thermal load of buildings all the while maintaining an

aesthetically pleasing and comfortable indoor environment. Advanced glazing can reduce the energy consumption of buildings by a trading off between lighting load costs and thermal loading costs of the building for better economic and environmental efficiency.

Electrochromic (EC) materials are one such type of advanced glazing materials that have been widely researched for their ability to change their thermal and optical properties based on the application of an external voltage. The determining factors for the use of EC's for advanced glazing depends upon several factors like the complexity and cost of manufacture, efficiency and speed of optical property change, and stability and durability under extreme environmental conditions. By studying the effects of different environmental conditions on the thermal and structural stability of the EC material, more efficient glazing materials can be designed.

The use of accurate computer simulations and modeling based on actual physical parameters increases the efficiency of studying such environmental effects. By specifying different parameters, computer applications can effectively predict what conditions are favorable and what conditions are not for the given type of EC material. This thesis describes one such technique for studying the characteristics of EC materials.

1.2 Problem Statement

The thermal and structural stability of EC materials is of prime importance for the successful use of such materials as an advanced glazing solution. The glazing has to withstand high temperatures of the summer as well as cold temperatures of the winter without compromising its structural integrity. Actual physical testing of glazing for such conditions requires the use of expensive equipment and a long time frame of

experimental observations. Computer based modeling is an effective way of simulating such extreme environmental conditions accurately and cost effectively without the long waiting times.

1.2.1 Methodology

This thesis discusses the use of the finite element analysis (FEA) software, COMSOL, for the study of the thermal and structural behavior of EC material on standard single pane and double pane glass structures. COMSOL divides the physical structure of the glass into multiple subdomains and evaluates the temperature and stresses occurring in each of the subdomains by solving the related differential equations. The input parameters like physical properties, initial temperatures and solar heat radiation values are used to solve the equations. This thesis examines the temperature and stress patterns for the glass structures for both time dependent and steady state conditions and tries to approximate the optimum usage and failure conditions for them. COMSOL 4.4 has been used for doing these studies in this thesis.

1.3 Motivation

Thermal and structural modeling of glass using computer software has been done by many researchers. However, to the knowledge of the author, there are only a handful of works done on this type of modeling with EC materials using FEA software. COMSOL is a remarkable software capable of simulating a variety of multiphysics problems using FEA techniques, but to the extent of our knowledge, the use of this software for glass coated with EC materials has not been done as of yet. Using COMSOL

to study the characteristics of EC coated glass under various conditions is the prime motivation of this research.

1.4 Objectives

The main objectives of this research are as follows:

- To create a model of EC material on double pane glass with the EC material on a particular surface of the glass panes.
- To simulate the conductive, convective and radiative heat transfers as well as structural stresses and deformations that occur on the models when subjected to solar radiation at different outdoor and indoor temperature conditions.
- To compare the temperatures and stresses on the glass pane models with and without EC materials.
- To evaluate optimal usage conditions and failure conditions for the models in terms of outdoor and indoor temperatures.

1.5 Limitations

This study is only involved in observing the effects of indoor and outdoor temperatures on Silica glass coated with EC materials and not on any other type of manufactured glass. It assumes that the effect of electrical heating caused by the application of a voltage on the EC layer is minimal and does not effectively contribute to the overall heating of the system. This study also does not account for the effects of rain and any other humidity factors on the glass system. The major assumption in this study is that the solar radiation is constant and at an angle perpendicular to glass pane, although in

real life, sunlight is irradiated at different angles at different times of the day and year on glass windows. The studies performed are steady state and so do not consider any time dependence in the results. Finally, the economic feasibility and ease of manufacture of different EC glazing systems are beyond the scope of this thesis.

1.6 Thesis Organization

This thesis consists of chapters differentiated by their respective topics. The first chapter is an introduction to the research work that has been done. The second chapter reviews different scientific papers pertinent to the study with a brief introduction of the basics of advanced glazing. The theories involved in heat transfer and structural mechanics is discussed along with an overview of the simulation models and procedures performed in COMSOL in Chapter 3. Chapter 4 consists of results of the simulations and Chapter 5 discusses these results. Chapter 6 summarizes the results and the research work in its entirety and references and appendices conclude this thesis.

Chapter Two: Literature Review

Before discussing the work being done on EC materials, we must first look at the different technologies that are employed in the field of advanced glazing and smart glass. For the purpose of keeping the radiative heat from indoors, low emissivity glass, known in the industry as low E glass, has been employed as well. This low E glass is highly reflective of solar thermal radiation energy in the infra red (IR) range and does not transmit much heat indoors without compromising much in the transmission of visible light. However, such windows cannot change their heat transmissivity dynamically and are only suitable for places that have high solar radiation all year long. Also, because this type of glass highly reflects solar heat, any concavity in the glass structure causes focusing of heat on the outside environment which might be harmful to people and structures on the outside of the windows. For this purpose, we will only consider glazing systems that can dynamically change their properties in terms of thermal and optical transmission.

2.1 Historical Background of Advanced Glazing

Advanced glazing, also known as Smart Glass, is a relatively new technology based on the changing of optical and thermal properties of the glass, like transmissivity of light, according to environmental conditions or the application of an external voltage.

Smart glass can be categorized according to the type of material used and the type of external stimulus that causes change in properties. The following are the important ones [**2**].

2.1.1 Thermochromic glazing

Thermochromic materials have the ability to change their optical properties depending upon their temperature [**3**]. Such materials have been used for glazing since the 1870's and their visible light transparency decreases with increase in the external temperature [**2**]. Current thermochromics under research consist of gels that are placed between the glass and a plastic which are clear when cold but become white translucent when hot [**2**]. Such types of glass are promising but have been known to leak gel material over time and are not commercially available as of yet [**2**].

2.1.2 Photochromic glazing

Photochromics are similar to thermochromics in that there is no need for manual control for the change in optical transmittance. However, photochromic materials change their properties reversibly depending upon the intensity of incident light as opposed to the external temperature [**4**]. Thus, photochromics are not dependent on the external temperature which is an advantage during the summer but a disadvantage during the winter when the solar radiation is required to contribute for indoor heating [**2**].

2.1.3 Liquid Crystal glazing

Liquid crystal glazing uses a modified form of liquid crystal display technology widely used in the wrist watch industry. In this type of glazing, a thin layer of liquid crystal materials is sandwiched between a pair of transparent conducting polymers such that the orientation of the liquid crystals change with the application of an Electric Field [**5**]. This assembly is known as Polymer Dispersed Liquid Crystal (PDLC) and it is this PDLC layer that gets laminated between two layers of glass [**2**]. The working principle of Liquid Crystal glazing is shown in figure 1 where the application of an external voltage causes the liquid crystals to align in a specific manner, allowing for the transmission of light. With the voltage removed, the crystals become arranged in random order and thus making the glass system translucent. The downside to this type of glazing though is that it requires a constant voltage supply (about 24 – 100V AC) for it to be transparent [**2**].

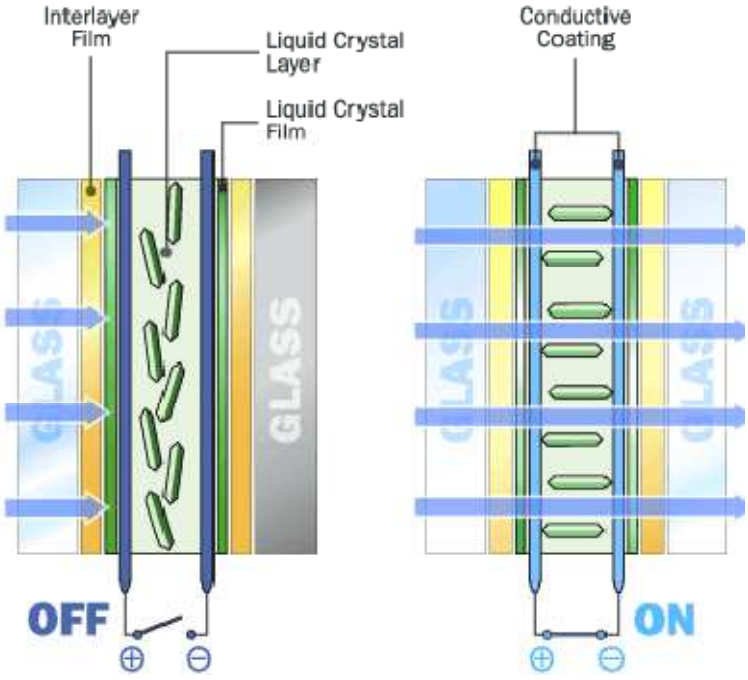

Figure 1. Liquid Crystal glazing working principle **[**2**]**.

2.1.4 Electrochromic glazing

Electrochromism is the ability of a material to reversibly change its optical transmission when it is electrochemically oxidized or reduced [**2**] [**6**] [**7**] [**8**] [**9**] [**10**]. Although EC materials were studied for their visible color change when they first emerged, these days the modulation of color researched upon includes wavelengths of light not visible to the human eye like the near IR, the thermal IR and microwave wavelengths [**6**]. EC materials have been commercially used mainly in three types of products: Windows, Displays and Mirrors [**6**]. EC windows have attracted recent interest due to their ability to tune the amount of light transmission as required. This has the advantage of lowering cooling costs as well as catering to comfort factors like glare and privacy [**6**].

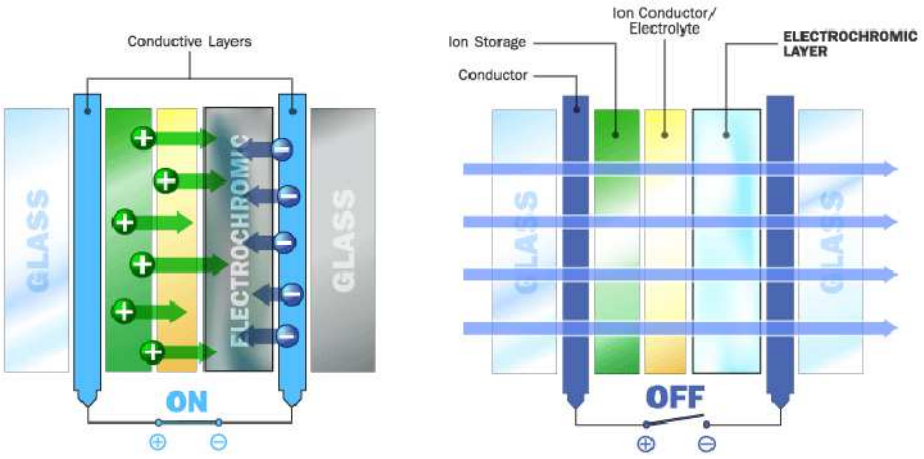

Figure 2. Structure and working principle of EC glass **[**2**]**.

One type of structure of EC glazing is shown in figure 2. For this type of EC glazing, the glazing consists of a pair of transparent conductive layers sandwiching the active EC material layers. The EC layers can be in three different forms, the battery-like,

the solution and the hybrid forms which will be discussed later [**6**] [**11**] [**12**]. The form shown in figure 2 is the battery like form. Here the EC layers consist of an active EC layer and a passive counter electrochromic (CE) layer with an ion conducting electrolyte layer in the middle. These layers are then laminated onto the glass layers. The application of a voltage causes ion migration from the active to the passive EC layers causing the whole system to become darker. Removing the voltage causes the reverse migration of ions causing the layers to become transparent. The type of EC material used determines different characteristics of the glazing such as speed of color change, thermal absorption, color of the tint etc.

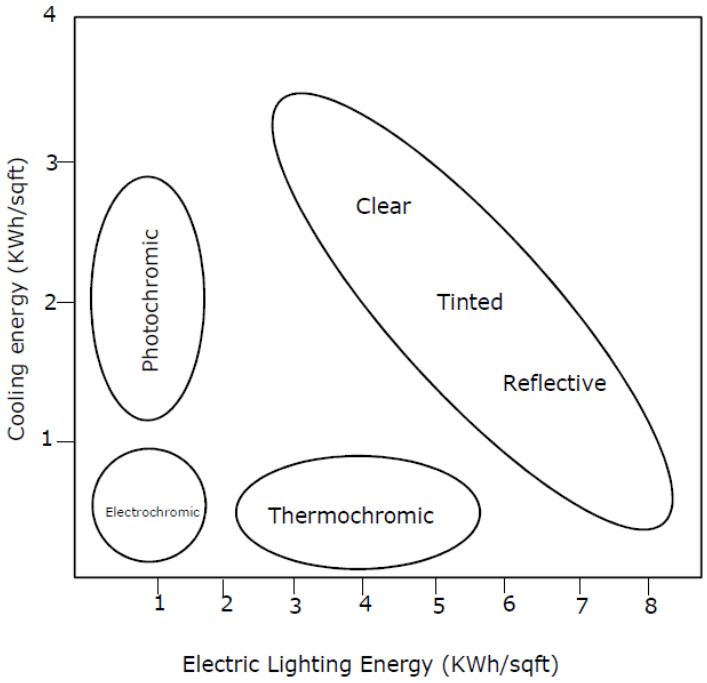

Figure 3. Conceptual comparison of cooling vs. lighting energies for different glazing types [**2**].

The tunability of tint and manual control of this tunability are the main advantages of EC glazing. This means that the lighting and cooling costs due to glazing can be controlled manually. Figure 3 shows a conceptual comparison of the relative cooling energy requirements versus lighting energy requirements for different types of advanced glazing systems and it is clear that EC glazing is the most energy efficient glazing among the other types of smart glass technologies.

2.2 Current EC technologies

The three configurations of EC layers that can be encapsulated into windows, as mentioned above, are the battery-like form, the solution phase form and the hybrid structure form as seen in figure 4 [**6**]. For all three configurations, the common feature is the presence of transparent conducting electrode layers on either side of the EC materials. These electrode layers are usually either a doped form of Tin Oxide (TO) or Tin doped Indium Oxide (ITO) and are seen as Transparent Conducting Oxide (TCO) layers in figure 4.

As discussed in the previous section, the battery-like configuration consists of thin films of EC and CE materials are coated onto the TCO's and the materials are separated by electronically insulating ion conducting electrolyte. The electrolyte can be in the form of a polymeric gel or a thin film [**6**]. If a thin film electrolyte is used, all layers are thin films and manufactured using thin film deposition technologies like sputtering or vapor deposition. On the other hand, polymeric gel type electrolytes are directly laminated onto glass. The solution configuration consists of the EC and CE materials dissolved in an

electrolyte in a solution. The hybrid configuration is a combination of battery-like and solution configurations as seen in figure 4.

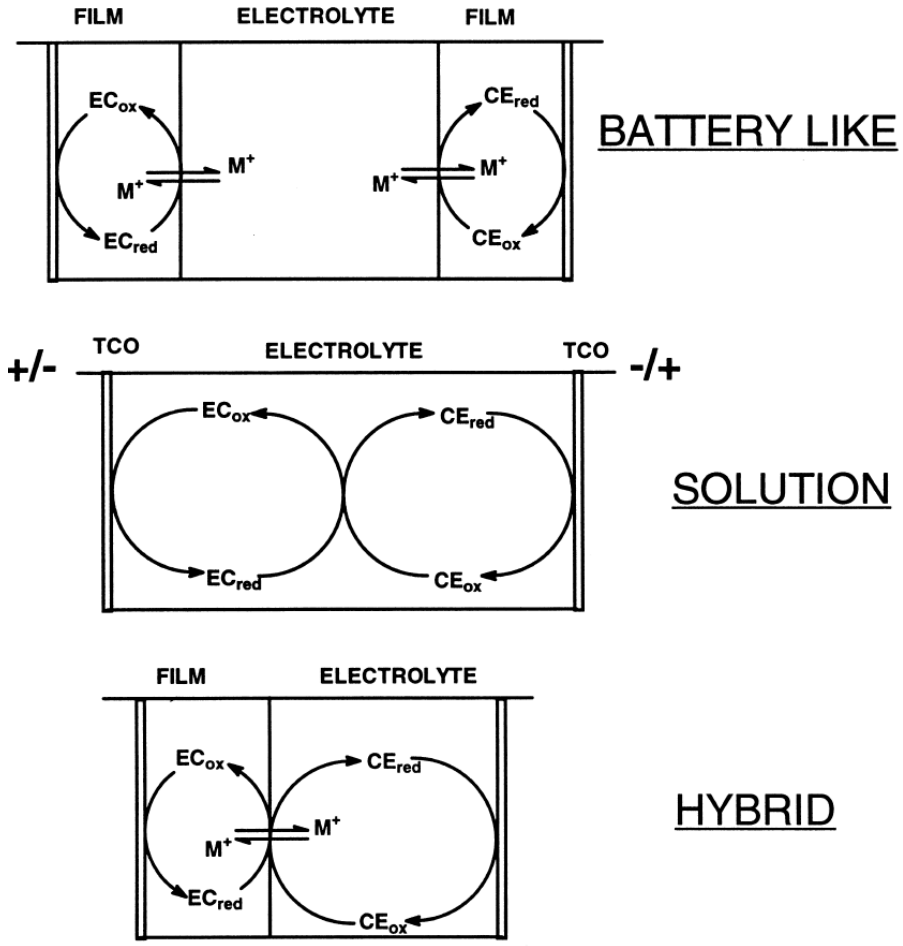

Figure 4. Three different configurations for EC windows **[**6**]**.

The hybrid and solution configurations are also known as self erasing configurations because either one or both of the color changing EC materials are dissolved in the electrolyte [**11**]. The application of a voltage causes the color of the EC

materials to change while its removal makes the EC materials dissolve in the electrolyte and make the window bleached.

Different chemical compounds can be used as the EC and CE materials. However, the basic stoichiometric equation that governs the working of EC windows requires charge balance between the two electrodes. Here the charge injected in the cathode half equation has to balance out the charge extracted in the anode half equation. Equation 1 shows the general redox reaction in EC windows such that the left hand side of the equation represents the bleached state and the right hand side represents the colored state [**6**].

$$EC^{n} + yCE^{m} \leftrightarrow EC^{n-a} + yCE^{m+(a/y)} \quad (1)$$

Here, n and m represent the oxidation states of the EC and CE materials respectively in the bleached state and y represents the possibility of the materials being present in any stoichiometric ratios [**6**]. Figure 4 shows this reaction as the EC and CE materials go from reduced states to oxidized states or vice versa. Figure 4 also shows that when one material is in the reduced state, the other material has to be in the oxidized state.

Electrochromic materials have to switch from high optical transmittance in the bleached state to highly absorptive in the colored state and this switching has to be consistently reversible as well. The total absorption of light of particular wavelength for an EC or CE in the bleached state depends upon the product of their respective absorption coefficients and thicknesses. The absorption in the bleached state also depends upon the coloration efficiencies of the layers and the proportion of residual charges left behind due

to incomplete redox reactions in the materials. The total combination of all these factors in a range of wavelengths determines the absorption of light in the bleached state which, in turn, determines the effectiveness of the EC glazing window. Different EC compounds have different values of absorptivity depending upon their structure and color. Discussed below are some of the compounds that are being researched in the present day.

2.2.1 EC's based on Metal Oxides

Oxides of metals, specifically of the transition metals, have been known to express a variety of colors. Such metals are known to have multiple oxidation states owing to the relatively low reactivity of the electrons in their outermost d shells. The electrons are able to transition within the d shells at different energy levels and it is this electron transition from higher to lower energy states that emits photons of different wavelengths depending upon the difference in the energy states. The ability to easily transition from one oxidation state to another with the introduction of electronic charge and the fact that transition metals can have multiple oxidation states in different crystalline forms mean that these metal oxides are ideal for chromatic modulation of visible light with electric currents. The actual electrochemistry and crystallography of transition metal oxides that causes the color changes is beyond the scope of this thesis. However, the properties and fabrication processes of some of these oxides will be briefly discussed below.

The efficiency of changing colors depends upon the ease of intercalation of the oxides which is the ability of the different metal ions to reversibly insert in between and

remove themselves from molecular crystalline oxide structures. Tungsten Oxide, generally represented as WO_3, is one of the most widely used metal oxides for EC windows [**13**] [**14**] [**15**] [**10**]. This is primarily because of its high intercalation efficiency, durability and color modulation efficiency in the visible range [**6**] [**16**] [**17**]. WO_3 is easily the most popular choice for the EC electrode in EC glazing windows also because of the ease of manufacture of electrodes with it [**6**].

Tungsten Oxide is often referred to as a cathodic EC material because the color-change from bleached to colored state occurs at the cathode or positive electrode through reduction [**18**]. Oxides based on Titanium (Ti), Molybdenum (Mo) and Niobium (Nb) are other cathodic EC materials that become colored due to charge insertion at the cathode [**13**] [**18**] [**19**]. Iridium (Ir) and Nickel (Ni) oxides are called anodic EC materials because their coloration occurs at the anode electrode due to charge extraction while oxides of Vanadium (V) can act as cathodic and anodic EC material depending upon the wavelength of light [**18**] [**19**]. Hexacyanometallates, metal compounds with six cyno groups, are also known to exhibit high anodic properties [**18**] [**20**].

Amorphous Tungsten Oxide (a-WO_3) is the most widely studies cathodic EC material with almost no serious competition from other metal oxides [**18**] [**21**]. This is due to the high up-scaling capability of depositing a-WO_3 through sputter deposition. WO_3 has been studied as an EC material since the 1930's although its color changing properties have been know since the early 19^{th} century. a-WO_3 changes its color from transparent to a dark blue color when small cations of Hydrogen (H), Lithium (Li) or Sodium (Na) are electrochemically inserted. The coloration is believed to be caused due

to the insertion of charge balancing. These electrons transition between localized states by absorbing light energy and thus causes light absorption and coloration [**18**]. WO_3 can have colors ranging from pale purple, blue and dark brown depending upon the ratio of W and oxygen present in the EC electrode [**18**].

The chemical reaction that causes this color change can be represented by the following equation:

$$WO_3 + xM^+ + xe^- \leftrightarrow M_xWO_3 \quad (2)$$

where, M can be H, Li or Na, e^- represents injected electrons and x is a stoichiometric parameter that can vary between 0 to 1 [**22**] [**23**] [**24**] [**25**]. The depth or darkness of color depends upon the value x or in other terms, the amount of charge or current injected. There are several theories about how this color change occurs. One such explanation is given by Lee *et al.* They propose that a-WO_3 layers consist primarily of W in the +6 and +4 states and the application of electronic charge transitions their state to the +5 state which causes the color change and optical absorption [**26**]. They verify this theory through Raman scattering measurements of the EC layers deposited with a-WO_3 that concludes the presence of W in the +4 and +6 states while bleached and in the +5 state when current is conducting through the layer and the layer is colored [**26**].

Fischer *et al.* used WO_3 as their primary EC electrode and a complimentary Ferric Ferrocyanide ($Fe[Fe(CN)_6]$), also known as Prussian Blue, as their anodic EC material in their paper that examines the solar and visible transmittance modulation by the use of EC materials in windows [**7**]. They also simulated the thermal characteristics of their design at certain solar exposures in the FEA software Abaqus Standard. This thesis uses some of

the parameters specified by their paper to simulate the structural and thermal characteristics of EC materials in COMSOL. Their design for the EC window can be seen in figure 5.

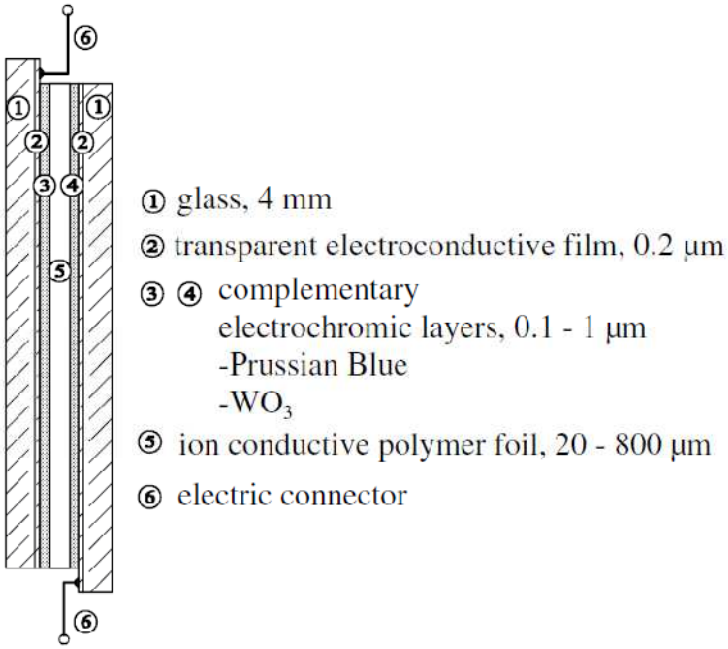

Figure 5. Structure of an EC window with WO_3 and Prussian Blue as EC materials [**7**].

Fischer *et al.* in their paper describe that the two complimentary EC materials become dark blue when a dc voltage between 1.2 to 2.4V is applied in the window system. The EC glazing has a calculated maximum visible light transmittance of 75% when bleached and 8% when fully colored with maximum reflectances of 9% and 6% for fully bleached and fully colored states respectively [**7**]. Similarly, the calculated solar transmittance ranges from 52% to 6% and the solar reflectance varies from 8% to 7% from bleached to colored states [**7**].

Kraft *et al.* also use the combination of Prussian Blue and WO_3 as their EC materials and investigate the light transmittance of their design of EC glass. The EC glass they study is a product of Gesimat, German smart glass manufacturing company. Their EC glass design has a battery-like configuration with Polyvinyl Butyral (PVB) as their polymer electrolyte [**9**]. Their finding conclude that the design has visible light transmittance from 77% to 8% and solar transmittance from 56% to 6% when transitioning between fully bleached to fully colored states [**9**].

Zheng *et al.* describe the properties, fabrication techniques and applications of nanostructured WO_3. These applications include EC windows, Solar cells, optical recording devices and sensing applications. They compare nanostructured WO_3 with bulk amorphous and crystalline WO_3 and conclude that nanostructured WO_3 has lower power consumption, higher coloration/bleach efficiency and faster coloration/bleach time than its amorphous and crystalline counterparts [**22**].

Recent works also suggest the use of monohydrous ($H_2O.WO_3$) and dihydrous (2 $H_2O.WO_3$) WO_3 as an EC material instead of the anhydrous WO_3 described above. Bessière *et al.* powdered $H_2O.WO_3$, which is more flexible than the anhydrous form, and obtained an infrared reflectivity ranging from 2% to 32% [**27**]. They reason that the Hydrogen bonding in the $H_2O.WO_3$ makes intercalation of Li ions in between the WO_3 crystals easier which causes the near total absorption of IR wavelengths [**27**]. Similarly, Liang *et al.* used nanosheets of $2H_2O.WO_3$ for their EC material on flexible plastic as the dihydrous WO_3 is more flexible than the anhydrous WO_3. They obtained higher

transparency contrasts, faster coloration/bleach times and higher coloration efficiencies when compared to anhydrous WO_3 EC materials [**28**].

Nickel Oxides are the next most widely used metal oxides for EC materials [**29**] [**30**]. Nickel Oxides are anodic and change color from transparent state to colored state when protons are extracted or hydroxyl ions are added, or in other words, the oxidation state is increased. Although not extensively researched, Ni Oxides in combination with Vanadium, Lithium and other metals have shown promising color modulation [**18**]. DC Magnetron sputtering is the most popular technique for deposition of Ni Oxides on glass with large industrial scalability with RF magnetron sputtering also being used to do the same [**31**] [**32**] [**33**]. The combination of WO_3 and Ni Oxides with each other and other metals has been researched and such combinations also have coloration features of their own. WO_3 with V and Mo has been known to create a more neutral color in the colored state [**34**]. Gold containing Ni oxides have attracted interest of recent researchers as well [**35**].

Lechner *et al.* demonstrated their use of WO_3 with V and a complimentary Ni Oxide as their EC material for their design of EC on glass and polymeric foils. They cite the difficulty in depositing such EC materials on polymeric foils to be due to the structural failure of such foils during the high temperatures involved in evaporation of those materials and use other techniques like reactive electron beam evaporation and DC magnetron sputtering instead [**23**]. They obtained a visible light transmittance change from 65% to 8% for their design with V and from 78.5% to 31% without V [**23**].

The usage of organic metal complexes and polymers has also gained some attention in EC research owing to their intense coloration and redox activity [**36**]. Organic compounds like thiophenes, dioxythiophenes, pyrroles, dioxypyrroles and other copolymers have been documented to display colors throughout the whole color spectrum in their colored states depending upon the compounds used [**36**]. Gao *et al*. successfully fabricated EC layers with Polyoxometalates (POM's), which are organic complexes of metals like Tungsten, Copper or Iron, and verified that such EC materials have low operational potential, good thermal stability and suitable response time [**37**]. The use of the conductive compound ethylenedioxythiophene (EDOT), that polymerizes to form polyethylenedioxythiophene (PEDOT) which forms highly anodic coloring films, was demonstrated to have very high coloration efficiency and subsecond color switching times by Sapp *et al* [**38**].

2.2.2 Thermal and structural modeling of EC's

The use of computer simulation models for studying glass and electrochromics is not a new area of research. To the author's knowledge, such simulations for studying thermal and structural characteristics of EC materials and specially the use of FEA software has been lacking however. Jonsson *et al.* studied the effects of different control strategies for optimization of energy usage for heating and cooling for different window configurations like double paned glass, double paned glass with EC layer, double paned glass with low-E glass etc [**8**]. They used the window energy balance simulation tool, Winsel, to calculate the contribution from the windows to the energy balance of the

building using parameters like solar radiation, thermal losses and solar gains and other window parameters for the climate conditions of Stockholm, Denver and Miami [**8**]. Their paper however is limited to the energy contributions of the window configurations and not the thermal and structural characteristics of the windows themselves. However, they conclude that their simulation results show that EC windows do indeed contribute in the overall energy efficiency of the building in terms of heating and cooling [**8**].

Similarly, Bahaj *et al.* also studied energy efficiencies of different advanced glazing technologies like EC glass, aerogel glazing, low-E glazing and the basic window blinds for different buildings in the Middle-East using a fenestration software created by the Lawrence Berkeley National Laboratory called Window [**39**]. Their studies conclude that permanently tinted EC glass can reduce the energy required for cooling purposes significantly better when compared to other window configurations, although such EC glass would produce blue light which is not aesthetically pleasing. However, a tint controllable EC glass theoretically can produce energy savings by up to 25% [**39**].

Piccolo used actual experimental setups and computer simulations to compare the thermal characteristics of a test cell with and without a WO_3 EC glazed window in real world weather conditions for a primarily warm climate for different orientations of the test cell. The computer simulation is done in FORTRAN-90 using a finite difference analysis technique using ambient temperature values obtained from direct measurements [**40**]. The EC glazed window has an automatic tint-control based on temperatures with the EC layer on the outside face of the glass. The paper concludes that the EC window rejects most of the heat from the solar radiation outwards with an average of 10% temperature

difference from the hotter outside surface to the cooler inside surface for west facing configuration with up to 50% energy savings for cooling purposes [**40**].

The use of FEA for analysis of the thermal and structural characteristics of EC materials, as to date, was done by Fischer *et al*. In addition to calculating the transmittance and reflectance of EC materials at the bleached and colored states, the group also simulated the temperature and stress profiles of a double pane glass with EC layer deposited as seen in figure 5, in the FEA software Abaqus Standard. Their paper evaluated these profiles for an 800W/m^2 solar radiation heat source that reduces to 696W/m^2 on the EC layer due to reflection and absorption by the transparent glass which ramps up to its maximum in and ramps down to zero within 20 minutes [**7**]. They simulated different shading conditions and for their heating profiles for outdoor and indoor temperatures of 10˚C and 20˚C respectively and concluded that the temperature of the glazing system does not go above 28.51˚C and the tensile stress does not go above 3.11×10^6 N/m^2 which is well within the limits of the glass tensile stress of 3.3×10^7 N/m^2 or 33MPa for glass [**7**].

Chapter Three: Methods

This research thesis is based on the use of COMSOL Multiphysics, an FEA software capable of modeling and solving different kinds of engineering and scientific problems. A brief introduction to the Finite Element Method (FEM) and COMSOL Multiphysics is given and the theory of the different heat transfer and structural mechanics modules used in this project are described before explaining the steps undertaken for the modeling of the problem at hand.

3.1 Finite Element Method

Finite element method or finite element analysis is a computational technique used to find the approximate solutions to boundary value problems in mathematical physics and engineering. Boundary value problem, sometimes referred to as field problems, has one or more dependent variables that have to satisfy a certain differential equation in all regions of a known domain and specific conditions or values at the boundary of the domain. FEM is useful in solving problems with complex geometries and large number of material property variables where analytical methods become too complicated or even impossible to apply. The geometrical complexity of the domain makes obtaining an exact closed-form solution extremely difficult to obtain. FEM uses numerical methods and computers to approximate the solutions with high accuracy [**41**].

The invention of FEM dates back to the aeronautical industry of the post World War II era where there was a need to solve complex structural analysis problems of spacecrafts, missiles and jets. With the enhancement of computational power of modern computers, FEM has found applications in several fields like Civil, Automotive, Aerospace and Mechanical Engineering for solving problems in heat transfer, fluid motion, electromagnetics, acoustics, soil mechanics etc [**42**]. In FEA, each domain is subdivided into smaller elements of specific geometric shapes like triangle or quadrilaterals. The values of the dependent variable at the vertices, or nodes, of each element is interpolated from the boundary values for them and each adjacent node is solved for the dependent variable using the same interpolation technique until the entire domain is solved for [**41**].

The division of a domain into smaller elements is known as meshing and the more the element, or finer the mesh, the closer is the solution converges to the exact solution. However, the finer the mesh, the greater will be the computation time. So optimization between the mesh refinement and solution time has to be done so as to improve resource efficiency without compromising accuracy.

The general steps in solving problems using FEA in a computer software environment are as follows:

3.1.1 Preprocessing

This step involves the definition of the problem to be solved. Preprocessing includes defining the geometric domain of the problem, the element types to be used, the

material properties and geometric properties of the elements, the meshing, the boundary conditions, the initial conditions and the solution method for the problem [**41**].

3.1.2 Solution

Once the problem has been defined and its solution method specified, the software uses FEA technique to evaluate solutions for all dependent variables and then uses these solutions to calculate additional derived variables as desired by the user.

3.1.3 Postprocessing

Postprocessing is the step that involves interpreting the solution. This step may include creating tables, graphs, 3D images, animations, color coded plots, comparisons with other data etc.

3.2 COMSOL Multiphysics

COMSOL Multiphysics is an FEM simulation software capable of solving a multitude of engineering and scientific problems. It is a multiplatform software package capable of interfacing with other applications like MATLAB and other CAD software applications. COMSOL has a flexible GUI for ease of access and can also be programmed using Java and MATLAB [**43**]. COMSOL has the ability to solve for different types of studies like steady state or transient, linear or non linear, Eigenfrequency or frequency response studies with a variety of postprocessing and visualization tools. Some examples of application areas in which COMSOL can be used

are Acoustics, Bioscience, Chemical reactions, Corrosion and corrosion protection, Diffusion, Electrochemistry, Electromagnetics, Fatigue analysis, Fluid dynamics, Fuel cells and electrochemistry, Geophysics and geomechanics, Heat transfer, Microelectromechanical systems (MEMS), Microfluidics, Microwave engineering, Optics, Particle tracing, Photonics, Plasma physics, Porous media flow, Quantum mechanics, Radio-frequency components, Semiconductor devices, Structural mechanics, Transport phenomena, Wave propagation etc [**43**].

COMSOL supports all forms of heat transfer i.e. Conduction, Convection and Radiation and solves for the temperature field of the model in question. COMSOL can couple the heat transfer module with other physics modules as well and can solve a wide array of problems like thermal stress, electric Joule heating, fluid mechanics and convective cooling etc. The research in this thesis is based on Thermal stress which is a combination of Heat Transfer and Structural Mechanics Physics modules. Within the Heat Transfer part of the model, the features used are Surface to Surface Radiation, Surface to Ambient Radiation, Conductive Heat Transfer in Solids and Fluids and Convective Cooling by ambient air. The Structural Mechanics part of the model includes Linear Elastic Expansion and Fixed Constraints. The end result of the model is a 3D temperature and stress profile. A brief theory related to heat transfer and structural mechanics of the model is given below.

3.2.1 Heat Transfer in COMSOL

The transfer of energy from due to temperature difference can occur in three ways – Conduction, where the transfer occurs due to vibrating particles of the medium, Convection, where the heat content is transferred by a moving fluid and Radiation, where the energy is transported by photons. The following are the major types of heat transfer used in this thesis.

3.2.1.1 Heat Transfer in Fluids and Solids

COMSOL bases its heat transfer by the first equation of thermodynamics also called the conservation of energy principle and the basic heat transfer equation in a fluid it uses is given by equation 3.

$$\rho C_p \left(\frac{\partial T}{\partial t} + (\boldsymbol{u} \cdot \nabla)T\right) = -(\nabla \cdot \boldsymbol{q}) + \tau : \boldsymbol{S} - \frac{T}{\rho}\frac{\partial \rho}{\partial T}\Big|_p \left(\frac{\partial p}{\partial t} + (\boldsymbol{u} \cdot \nabla)p\right) + Q \qquad (3)$$

where, ρ is the density (SI unit: kg/m^3), C_p is the specific heat capacity at constant pressure (SI unit: J/(kg·K)), T is the absolute temperature (SI unit: K), $\boldsymbol{u}$ is the velocity vector (SI unit: m/s), $\boldsymbol{q}$ is the heat flux by conduction (SI unit: W/m^2), p is the pressure (SI unit: Pa), τ is the viscous stress tensor (SI unit: Pa), $\boldsymbol{S}$ is the strain-rate tensor (SI unit: 1/s) given by $\boldsymbol{S}$ = ½ ($\nabla\boldsymbol{u}$+($\nabla\boldsymbol{u}$)^T) and Q contains heat sources other than viscous heating (SI unit: W/m^3) [**44**]. Equation 3 is based on the conservation of mass assumption which means the relation between the density and velocity vector is given by $\frac{\partial \rho}{\partial t} + \nabla(\rho \cdot \boldsymbol{u}) = 0$. Fourier's law of heat conduction is used such that the conductive heat flux, q, is proportional to the temperature gradient given as: $q = -k\frac{\partial T}{\partial x}$, where k is the thermal conductivity in the x direction [**44**]. The second term on the right hand side of equation 3

represent viscous heating in the fluid and the third term represents pressure work. Ignoring these two terms, equation 3 is simplified to:

$$\rho C_p \frac{\partial T}{\partial t} + \rho C_p (\boldsymbol{u} \cdot \nabla) T = \nabla (k \nabla T) + Q \tag{4}$$

For no velocity vector value, equation 4 reduces to the following:

$$\rho C_p \frac{\partial T}{\partial t} + \nabla \cdot (-k \nabla T) = Q \tag{5}$$

Equations 4 and 5 solve for the temperature of the fluid in the Heat transfer in fluids module of COMSOL [**44**]. This equation is also applicable in solids as there is no velocity vector value for solids.

3.2.1.2 Radiation Heat Transfer in COMSOL

Equations 3, 4 and 5 do not represent radiation heat transfer. For a point $\overline{x}$ on the surface of a material with emissivity, ε, reflectivity, ρ, absorptivity, α, temperature, T, total incoming radiative flux or irradiation, G, and total outgoing radiative flux or radiosity, J, the schematic of radiation heat transfer is shown in figure 6.

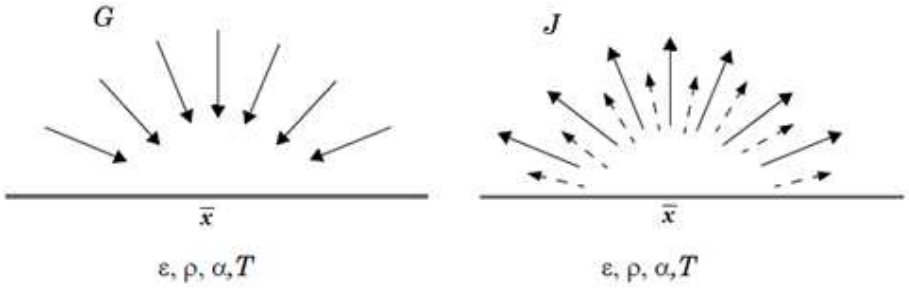

Figure 6. Basic mechanism for radiation heat transfer [**44**].

For an opaque material, J has to equal the sum of emitted and reflected radiation as represented by equation 6 where σ is the Stefan-Boltzmann constant = 5.670373×10^{-8} W m^{-2} K^{-4}.

$$J = \rho G + \varepsilon \sigma T^4 \quad (6)$$

The difference of *G* and *J* gives the net inward heat flux, *q*, and so, using equation 6, *q* can be written as:

$$q = (1 - \rho)G - \varepsilon \sigma T^4 \quad (7)$$

For ideal gray bodies, the absorptivity and emissivity are equal, which is the case for most opaque materials and so, the reflectivity can be found as α = ε = 1- ρ which reduces equation 7 to:

$$q = \varepsilon(G - \sigma T^4) \quad (8)$$

Equation 8 is used as the radiation boundary condition in COMSOL [**44**].

This thesis uses two types of surface radiation modules available in COMSOL – Surface to Surface Radiation and Surface to Ambient Radiation. The surface to surface radiation feature implements the radiosity method which assumes that the emissivity and absorptivity of the surface is independent of the angle of emission and absorption and assumes that the energy transfer between boundaries and heat sources does not involve any participation of the medium [**44**]. COMSOL also has a feature that enables the incorporation of wavelength dependence on emissivity and absorptivity values. This is because although surfaces that radiate at a limited temperature range do not have much wavelength dependence on emissivity, those that radiate over a large temperature range do indeed have that dependence which is true for solar radiation. For surface to surface radiation in COMSOL, the irradiation *G* for equation 6 is the sum of the mutual irradiation arriving from other surfaces, the irradiation from external sources and the irradiation coming from ambient conditions [**44**].

In the case of surface to ambient radiation, COMSOL assumes that the ambient surroundings have a constant ambient temperature, T_{amb}, and the surroundings behave like a blackbody, i.e. the emissivity and absorptivity are equal to 1 and the reflectivity is equal to 0 [**44**] such that $G = \sigma(T_{amb})^4$ which reduces equation 8 to:

$$q = \varepsilon\sigma(T_{amb}^4 + T^4) \tag{9}$$

3.2.2 Thermal Stress and Solid Mechanics in COMSOL

COMSOL combines Heat Transfer and Solid Mechanics physics for the Thermal Stress interface. The temperature from the Heat Transfer physics of the model acts as a thermal load for the Solid Mechanics physics which causes appropriate thermal expansion or contraction [**45**]. The thermal stress interface solves for the stress and displacement due to thermal expansion. COMSOL requires the definition of the Young's modulus, E, and the Poisson's ratio, υ, of each material to calculate the stresses, strains and deformations due to thermal expansion. The expansion is dependent upon the coefficient of thermal expansion, α, which needs to be specified for this purpose. The temperature inputs for the thermal expansion are supplied by the heat transfer interface that is coupled with the solid mechanics interface in the thermal stress module. For the purpose of this thesis, the stress and temperature profiles of the Double glazed window configuration with an EC layer will be studied.

3.3 Model Definition in COMSOL

As explained before in section 3.1, the problem was defined in the preprocessing step of FEA using COMSOL. 3D studies were performed on two models of Double pane glass windows. The first was a standard double pane glass window without an EC layer and the second was a standard double pane glass window with an EC. In the glass industry, the outermost surface of a double pane glass, which faces the outside environment, is called surface 1, the inner surface of the outer glass pane is called surface 2, the outer surface of the inner glass pane is called surface 3 and the inner surface of the inner glass pane, which faces the interior environment, is called surface 4. For the model with the EC layer, the EC layer is coated on surface 2. For both cases, the gap between the two panes of glass, or surface 2 and 3, is filled with air and an aluminum spacer surrounding the entire structure to prevent the air from leaking out. The simulations done were for steady state conditions and so, there weren't any time variation considerations in the models. In order to define the models described above, the following six preprocessing steps were performed in COMSOL.

3.3.1 Parameter definition

The first step for modeling the problem is the definition of the parameters involved. Although this step is not always necessary for simpler model, the creation of a parameter list allows for the use of symbols of the different parameters instead of their actual values at different stages of the modeling. The parameters defined in this list can be used in the solver definition step for doing a sweep of the values of the required

parameters. For both models, the parameters defined in the list were of the geometric properties of the models and the indoor and outdoor temperatures for the model. The list of parameters used in the models is tabulated in Table 1. All the values for the parameter list were obtained from Fischer *et al.*'s paper "Heat Transport and Thermal Expansion of Electrochromic Glazing Systems Due to Solar Irradiation" and the specification sheet from Solaglas Ltd. Entitled "Window Energy Ratings data for double glazed unit specifications from Solaglas Ltd." [**7**] [**46**].

Table 1. *Parameter list for the models*

Name	Value	Unit	Description
t_g	4	Mm	Glass Thickness
l_g	42	in	Glass Length
w_g	28	in	Glass Width
T_o	20	˚C	Outside Temperature
T_i	20	˚C	Inside Temperature
t_ec	200	µm	EC layer Thickness
t_s	16	mm	Spacer thickness
w_s	6.5	mm	Spacer width

3.3.2 Geometry definition

After defining the parameters, COMSOL can reference the values in the parameter list to build the geometries in the model. The entire model was defined in terms of blocks of different dimensions as per the parameter list. The two glass layers had the dimensions of glass thickness, glass length and glass width. For the model with the EC layer, a block of the same length and width as the glass but with the EC layer thickness was created under the outward-facing glass layer. A hollow aluminum spacer

block of the same length and width as the glass blocks and height of spacer thickness and thickness of spacer width was built. The structures of the models are shown in figures 7 and 8. Figure 7 shows the model without the EC layer and figure 8 shows the model with the EC layer. Part a of the figures show the structure when the aspect ratio is preserved, part b of the figures show the structure when the aspect ratio is not preserved, and part c of the figures show the structure with transparency and without aspect ratio preservation. As the EC layer thickness is in the order of hundreds of micrometers while the glass thickness is in the order of millimeters, the EC layer becomes difficult to see when the aspect ratio is preserved. This is the advantage of removing the aspect ratio preservation so as to see and work with components like the EC layer whose dimensions might be too small to observe in normal view. From figures 7 and 8, the two layers of glass can be distinguished in the normal view and the view without aspect ratio preservation. The hollow nature of the aluminum spacers can be seen in the transparent views. The EC layer however can only be distinguished in the figure without the aspect ratio preservation.

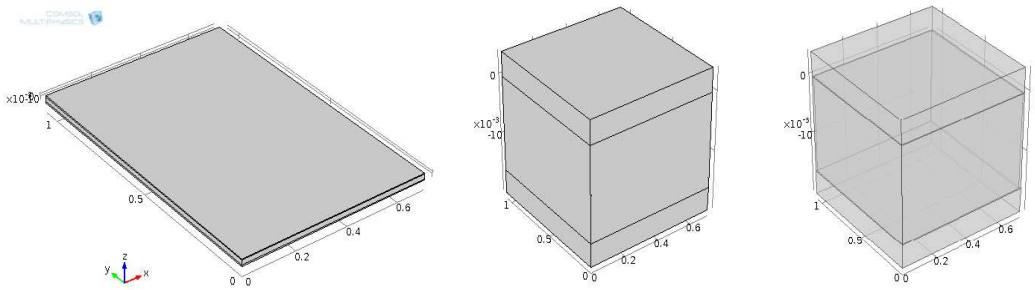

Figure 7. Structure of model without EC layer with a) aspect ratio preserved, b) aspect ratio not preserved and c) aspect ratio not preserved with transparency.

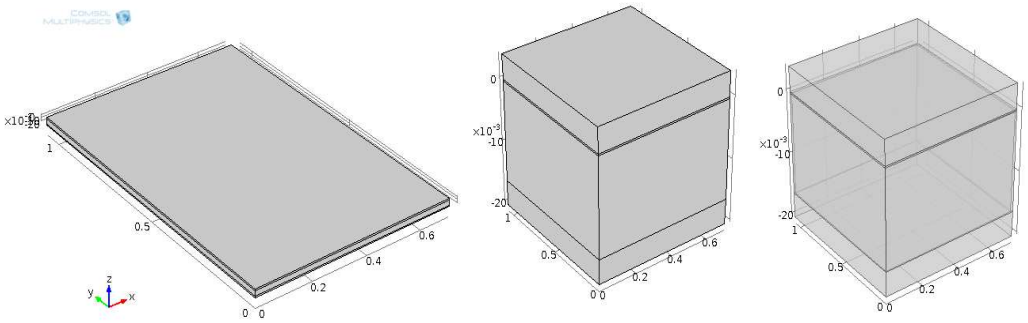

Figure 8. Structure of model with EC layer with a) aspect ratio preserved, b) aspect ratio not preserved and c) aspect ratio not preserved with transparency.

3.3.3 Material definition

After defining the geometries, each domain was specified its material properties. The material properties for the glass and EC layers were obtained from Fischer *et al.*'s paper. The material properties for air and aluminum were used from the built in material properties library of COMSOL. The surface emissivities for aluminum and glass were set to be 0.84 and 0.09 respectively. In the case of the EC material, based on the data from Fischer *et al.*, the visible wavelength emissivity was set to 0.87 while the IR wavelength emissivity was set to 0.86 [**7**]. The surface emissivity for all these materials were described during the physics definition step instead of material definition step because emissivity is a property of a surface not the entire material volume and can be defined when the physics requires it. COMSOL automatically asks for the material properties associated with the required physics involved. The material properties required for this simulation for silica glass, EC material and aluminum are given in table 2. The properties for air that were used were heat capacity at ratio of specific heats, constant pressure,

density and thermal conductivity. The ratio of specific heats for air is 1.4 while the rest of the properties all depend upon the temperature. COMSOL has a built-in database for this temperature dependence of the properties and lists out the exact values of the properties in equation forms with respect to temperatures. In the case of convective cooling due to air, the convective heat flux coefficients are defined in the physics definition step. For the outside air this value was taken to be 28W/(m^2.K) and for indoors it was set to 15W/(m^2.K). The value of 28W/(m^2.K) corresponds to wind speeds of about 10-11mph and the 15W/(m^2.K) value corresponds to air speeds of about 0.5mph.

Table 2. *Material properties used for silica glass, EC material and aluminum*

Material Property	Symbol	Unit	Silica Glass Value	EC Material Value	Aluminum Value
Coefficient of thermal expansion	α	1/K	8.2×10^{-6}	120×10^{-6}	23×10^{-6}
Heat capacity at constant pressure	C_p	J/(kg.K)	720	1000	900
Density	ρ	kg/m^3	2350	900	2700
Thermal conductivity	k	W/(m.K)	0.81	0.25	238
Young's Modulus	E	Pa	70×10^9	1.5×10^6	70×10^9
Poisson's ratio	υ	1	0.23	0.49	0.33

3.3.4 Physics definition

The physics involved in the model were defined after the material property definitions were completed in COMSOL. The Thermal Stress interface was selected in the physics definition section of the COMSOL model wizard. Selecting this interface

automatically combines the Solid Mechanics and Heat Transfer in Solids modules already present in COMSOL.

For the solid mechanics interface, the default nodes were the Linear Elastic Material node, the Free node and the Initial values node. In the Linear Elastic Material node, the linearly elastic materials domains which were glass, EC material and aluminum, were selected. COMSOL has the option to have an initial deformation and stress to the model but for the case of this research, there were none and so, the Initial values node had all the initial stress and initial deformations set to zero. A new Fixed Constraints node was added to the solid mechanics interface to simulate the fixed nature of a double pane glass set in a window frame. All the edges of the system except for the surfaces 1, 2, 3, 4 of the double pane glass and the inner aluminum surfaces were set to the fixed constraints node. Once these surfaces were set as fixed, the free node automatically changed these surfaces as overridden to be fixed instead of free.

For the heat transfer in solids interface, the default nodes were the Heat Transfer in Solids node, the Thermal Insulation node, and the Initial Values node. The heat transfer in solids interface has options for Surface to Surface Radiation which when selected allows for the use of and External Radiation Source as well as a Wavelength dependency of Emissivity. Both of these options were selected so that different emissivity values could be given for visible wavelengths and IR wavelengths for the EC material. In the Heat Transfer in Solids node, all domains except for the air domain were selected as air is not a solid. Inside this node, the EC material and Aluminum domains were selected to be opaque while the glass and air domains were set to be transparent to

all wavelengths of radiation. Also the initial temperatures of the entire system were set to be at 20˚C in the Initial values node.

A new External Radiation Source node was added to the heat transfer interface with a radiation source located at infinity with a direction perpendicular to surface 1 and a radiation intensity of 800 W/m^2. Surface to Surface radiation nodes were also added for the EC material surface and the inner surfaces of the aluminum to simulate surface to surface radiation occurring in between the two glass panes. The surface emissivity values for the materials were specified in these nodes. Finally, two Convective Heat Flux nodes were added to simulate convective cooling of the glass surface exposed to moving air i.e. surfaces 1 and 2. The convective heat coefficients were defined in these nodes. Based on these definitions, COMSOL automatically made all the external surfaces of the double pane system except for the two glass surfaces open to air as thermally insulated in the Thermal Insulation node. This is true because all surfaces in contact with the window frame are thermally insulated while the other surfaces aren't.

3.3.5 Mesh definition

The next preprocessing step for the modeling was defining the meshing for the system. For both the EC and non-EC cases, the first mesh definition made was creating a triangular mesh on surface 2 of the double pane glass structure. This triangular mesh structure was swept onto the rest of the materials involved by using the Swept meshing option. For each domain, the swept meshing was distributed into divisions using the Distribution option. The glass domains were distributed into 6 divisions each, the

aluminum domain was distributed into 10 divisions and the EC domain was distributed into 3 divisions as shown in figure 9.

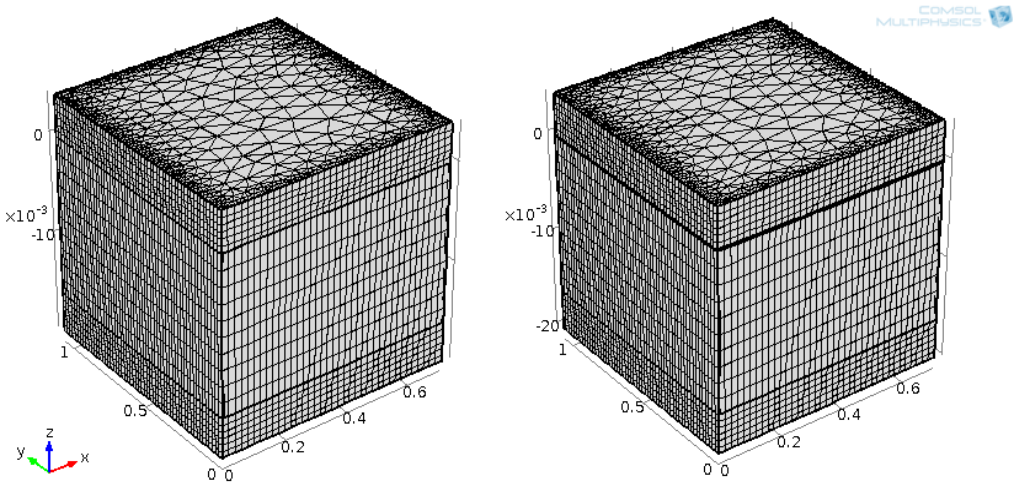

Figure 9. Meshing for Double pane glass without EC layer and with EC layer.

3.3.6 Solver definition

The final preprocessing step was the definition of the solver. The type of solver chosen was the Stationary Solver which is a steady state analysis of the model. The variation of dependent variables with respect to time is not calculated in the Stationary Solver as it only calculates the final steady state values. COMSOL provides the option to use a solver that either solves for the dependent variables separately with respect to the physics involved called the Segregated Solver, or solves for all the dependent variables at once called the Fully Coupled Solver. In the case of this research, the physics involved are Heat Transfer in Solids and Solid Mechanics and the solver used was the Fully Coupled Solver. Different types of methods can be used for the fully coupled solver and

the PARDISO method was chosen for this model. Finally, a parametric sweep for the external ambient temperature for surface 1 and the internal ambient temperature for surface 4 was set in order to simulate the different environmental temperatures the double pane glass might face. The external temperature sweep was set from -15˚C to 45˚C in 10˚C steps while the internal temperature sweep was set from 15˚C to 25˚C in 5˚C steps.

Chapter Four: Results

After the preprocessing steps were completed, the models were simulated and COMSOL solved for the dependent variables for the models which were temperature, stress and deformation. For the purpose of this research, the deformation was not important as only the temperatures and stresses were of interest. As mentioned before, the models in question were for a standard sized double pane glass with and without an EC layer on surface 2, the inner surface of the outer glass pane. COMSOL solved for the dependent variables for an external radiation source of intensity 800W/m^2 with the outdoor temperatures ranging from -15˚C to 45˚C and the indoor temperatures ranging from 15˚C to 25˚C.

Once the simulations were completed, COMSOL by default gave a 3D image of the models for temperature and stress profiles. The solutions for all the variables at different input parameter values of ambient temperatures were automatically stored in the model files. Different postprocessing techniques are available in COMSOL for analyzing the results like surface and volume average calculations, arrow plots, rainbow color plots etc. For the purposes of this thesis, the surface maximum and average values of temperatures and von Mises stresses were calculated for surface 1 and surface 4 of the double pane glass with and without the EC layer. The data obtained were tabulated and the differences in the average and maximum values for temperatures and stresses due to

the addition of the EC layer were calculated. The percentage differences in the dependent variables were then plotted in MATLAB.

As shown in figures 7 and 8, the view of the window with its actual dimensions does not fully demonstrate the full structure of window as the thickness is small in comparison to the length and breadth. Similar to those figures, the orthographic view of the window with the aspect ratio not preserved for different configurations are presented below. The transparent orthographic views are also shown in order to picture the internal stress and temperature profiles for the window configurations. The following figures are a sample of the data sets obtained by COMSOL for all the ambient temperature configurations done for the purpose of the research. The figures that follow are for the temperature and von Mises stress profiles when the outdoor temperature is 45˚C and the indoor temperature is 15˚C. The temperature and stress profiles for the rest of the ambient temperature conditions are very similar to the ones shown in these figures. These figures represent the hot extreme of the ambient temperature range that has been simulated for the purposes of this thesis.

Figure 10 shows the temperature profile of the double pane glass without the EC layer for outdoor temperature of 45˚C and indoor temperature of 25˚C. The transparent view of the window is also shown in the same figure. Similarly, figure 11 shows the von Mises stress profile of the non-transparent and transparent views of the double pane glass for the same conditions. Figures 12 and 13 show the temperature and stress profiles for the same temperature configurations for the double pane window with the EC layer on surface 2.

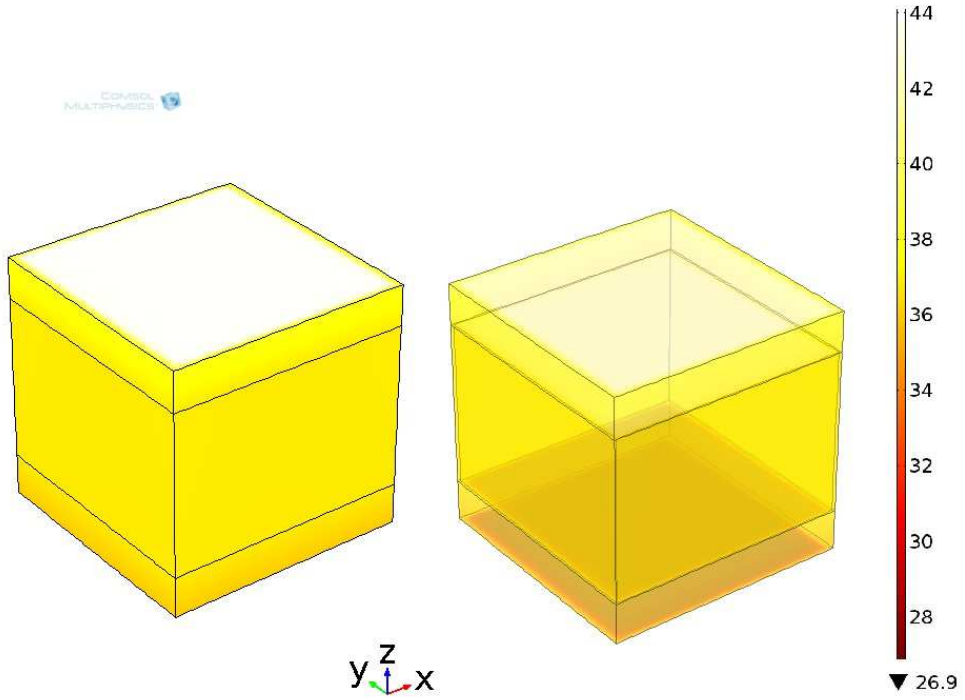

Figure 10. Temperature profile of double pane glass without the EC layer.

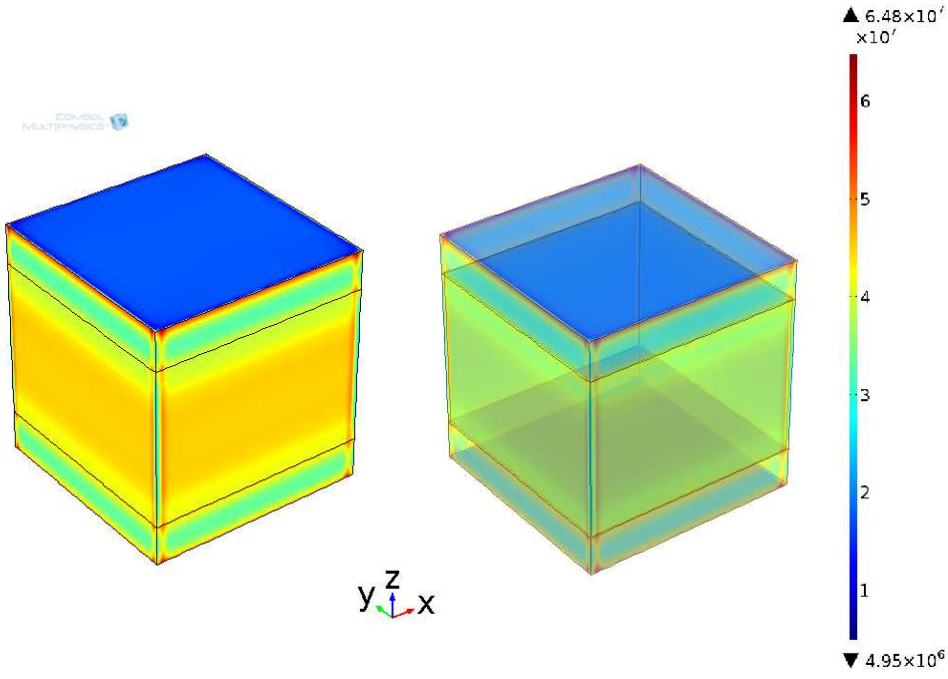

Figure 11. Stress profile of double pane glass without the EC layer.

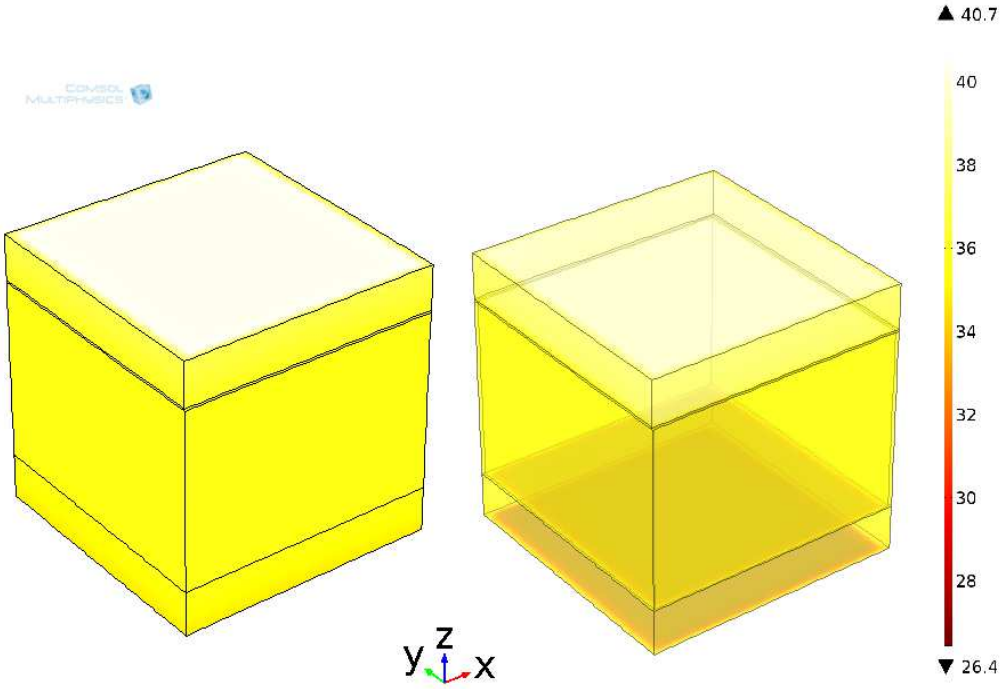

Figure 12. Temperature profile of double pane glass with the EC layer.

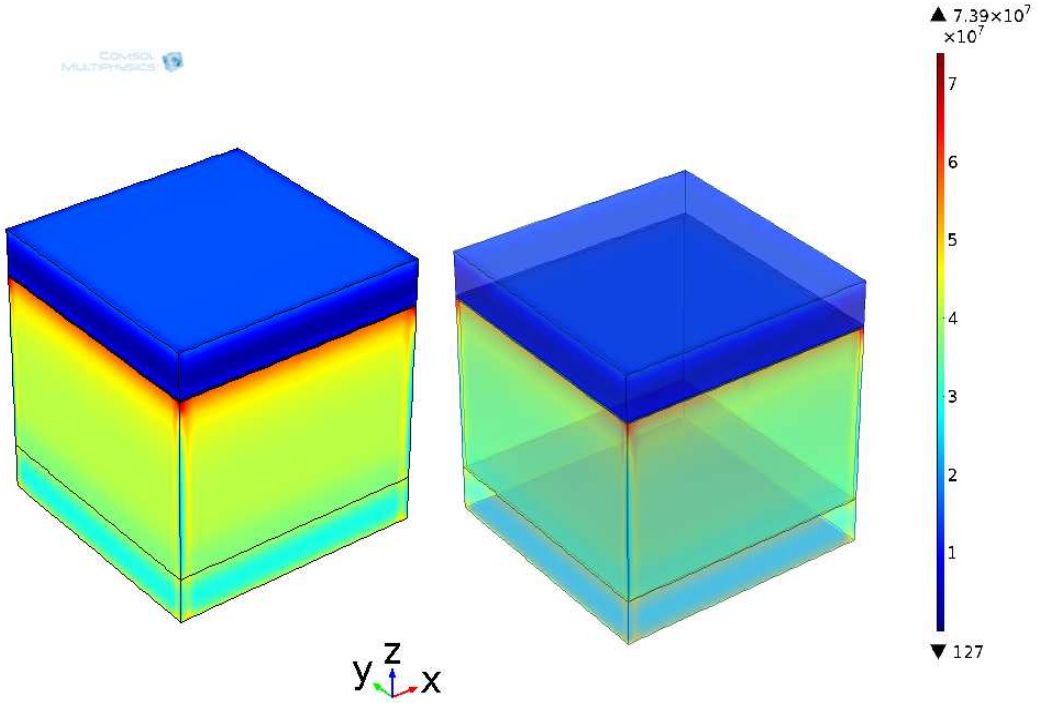

Figure 13. Stress profile of double pane glass with the EC layer.

Additionally, figure 14 shows the direction of the principal stresses experienced by surfaces 1 and 4 in the three coordinate-axis directions for the double pane glass configuration with an EC layer on surface 2. The von Mises stress calculated by COMSOL is a resultant of these principal stresses. From top to bottom, the principal stresses are in the z, x and y directions respectively. This type of stress direction profile is common for all glass configurations and ambient temperature combinations.

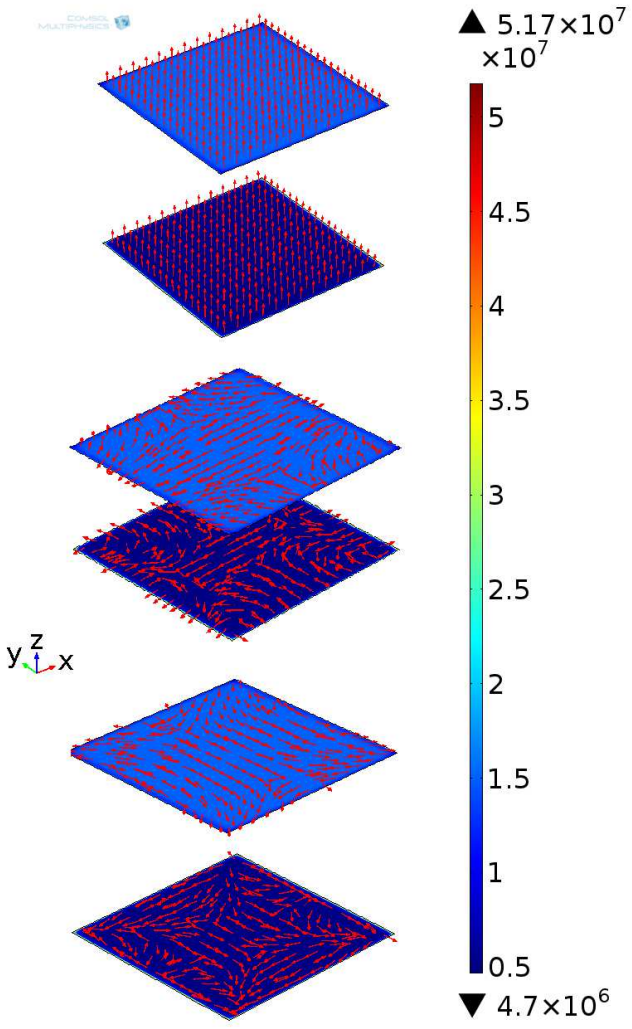

Figure 14. Direction of principal stresses in the z, x and y directions for double pane glass with EC layer.

Table 3. *Percentage difference in maximum surface temperatures and von Mises stresses on surfaces 1 and 4 due to addition of EC layer.*

Ambient Temperatures		Percentage Difference		Percentage Difference	
T_o/˚C	T_i/˚C	T1/%	T4/%	S1/%	S4/%
-15	15	25.296	3.340	-73.229	-10.727
-5	15	35.903	2.395	-73.769	-10.718
5	15	6.099	1.447	-74.780	-10.501
15	15	4.223	1.708	-76.870	-9.348
25	15	-2.282	-0.829	-49.241	-3.091
35	15	-5.452	-2.348	-68.680	-14.106
45	15	-7.420	-3.404	-70.580	-13.439
-15	20	40.962	2.430	-71.989	-11.282
-5	20	18.377	1.766	-72.101	-11.467
5	20	4.375	1.077	-72.214	-11.656
15	20	0.932	0.364	-72.327	-11.848
25	20	-2.511	-0.948	-72.441	-12.043
35	20	-5.609	-2.343	-72.556	-12.240
45	20	-7.542	-3.346	-72.670	-12.440
-15	25	139.667	1.905	-70.502	-11.956
-5	25	11.593	1.394	-69.946	-12.457
5	25	3.162	0.852	-68.267	-13.507
15	25	0.444	0.281	-48.975	-3.111
25	25	-1.134	-0.317	-76.933	-9.560
35	25	-5.766	-2.342	-75.074	-11.092
45	25	-7.665	-3.297	-74.287	-11.694

Figures 10 through 13 depict the general temperature and von Mises stress distributions for the two glass configurations. To gain a more quantifiable understanding of these profiles, the maximum and average temperature and von Mises stress values for surfaces 1 and 4 were tabulated in COMSOL in the postprocessing step using the built in Surface Maximum and Surface Average functions. The percentage difference in temperature and stresses caused by the addition of the EC layer was then calculated from the tabulated values. Table 3 shows the percentage difference in the maximum surface

temperatures and von Mises stresses for surfaces 1 and 4 due to addition of the EC layer while table 4 shows the percentage difference in the corresponding average values. For both tables, T_o and T_i represent outdoor and indoor temperatures, T1and T4 represent temperatures on surfaces 1 and 4 and S1 and S4 represent von Mises stresses on surfaces 1 and 4 respectively. The original data from which these two tables are derived from are included in Appendix A.

Table 4. *Percentage difference in average surface temperatures and von Mises stresses on surfaces 1 and 4 due to addition of EC layer.*

Ambient Temperatures		Percentage Difference		Percentage Difference	
T_o/˚C	T_i/˚C	T1/%	T4/%	S1/%	S4/%
-15	15	29.611	4.549	-12.426	-5.901
-5	15	79.321	3.090	-12.854	-5.259
5	15	30.978	1.789	-13.308	-4.093
15	15	4.271	0.606	-13.900	-1.932
25	15	-2.343	-0.487	-13.724	1.922
35	15	-5.536	-1.509	-14.386	5.410
45	15	-7.534	-2.476	-14.859	9.743
-15	20	30.178	3.236	-12.397	-10.543
-5	20	87.035	2.253	-12.810	-11.004
5	20	28.461	1.322	-13.227	-11.473
15	20	3.883	0.432	-13.648	-11.951
25	20	-2.501	-0.424	-14.074	-12.436
35	20	-5.626	-1.254	-14.503	-12.928
45	20	-7.594	-2.061	-14.933	-13.427
-15	25	30.781	2.499	-12.367	6.732
-5	25	96.775	1.760	-12.761	6.398
5	25	26.207	1.035	-13.137	4.338
15	25	3.507	0.321	-13.322	1.823
25	25	-2.656	-0.385	-14.354	-2.036
35	25	-5.715	-1.083	-14.611	-4.707
45	25	-7.655	-1.776	-15.005	-6.578

The data from tables 3 and 4 were then used to make graphs that better illustrated the percentage changes in the dependent parameters of surface 1 and 4 due to the presence of the EC layer. Figures 15 through to 18 show the percentage changes in the surface maximum temperatures and von Mises stresses for surfaces 1 and 4 while figures 19 to 22 show the percentage changes in the surface average temperatures and von Mises stresses for surfaces 1 and 4.

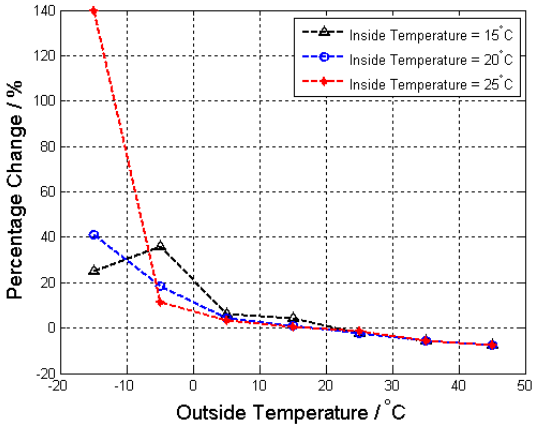

Figure 15. Percentage change in maximum surface temperatures for surface 1.

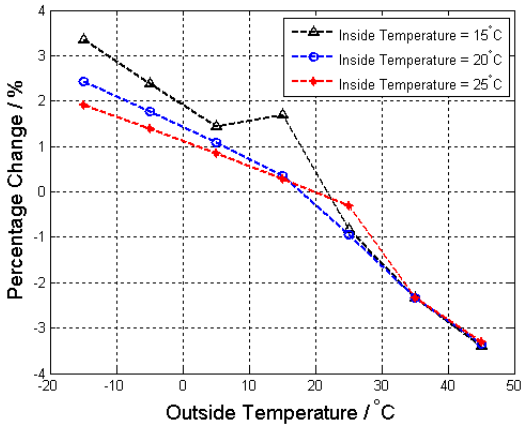

Figure 16. Percentage change in maximum surface temperatures for surface 4.

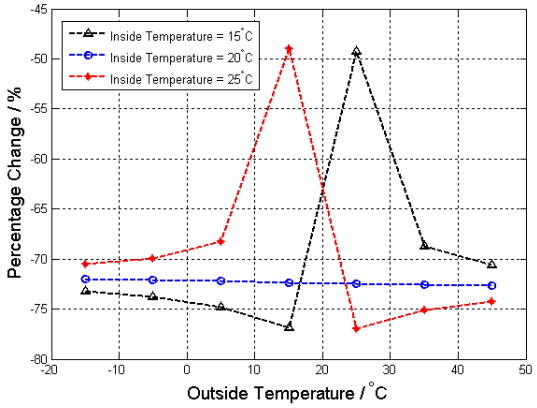

Figure 17. Percentage change in maximum surface von Mises stress for surface 1.

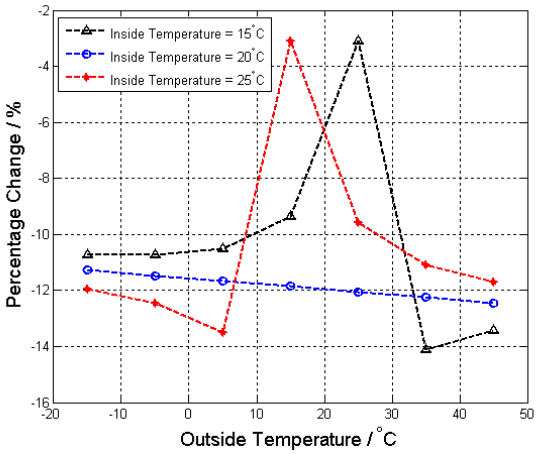

Figure 18. Percentage change in maximum surface von Mises stress for surface 4.

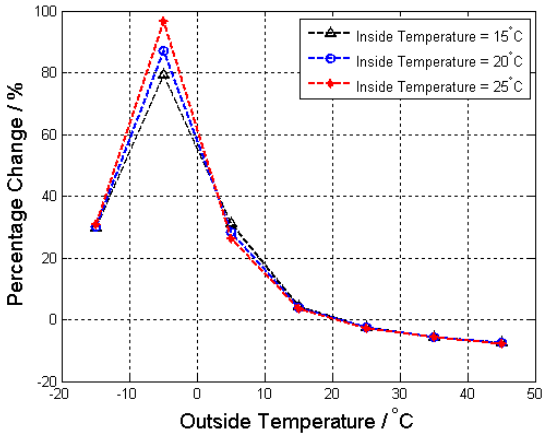

Figure 19. Percentage change in average surface temperatures for surface 1.

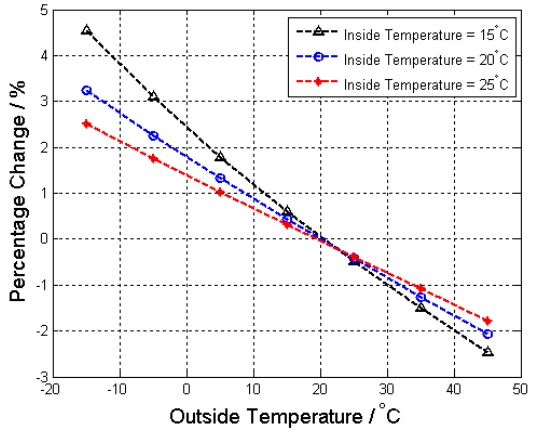

Figure 20. Percentage change in average surface temperatures for surface 4.

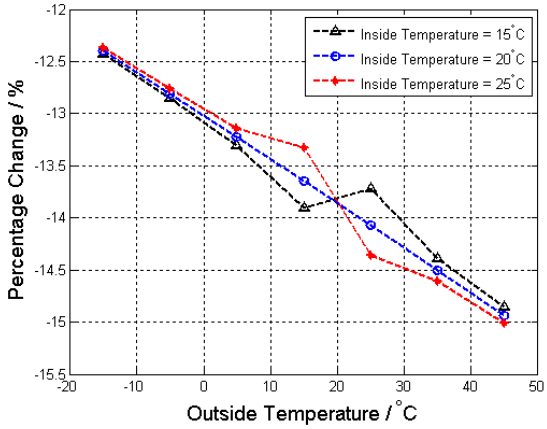

Figure 21. Percentage change in average surface von Mises stress for surface 1.

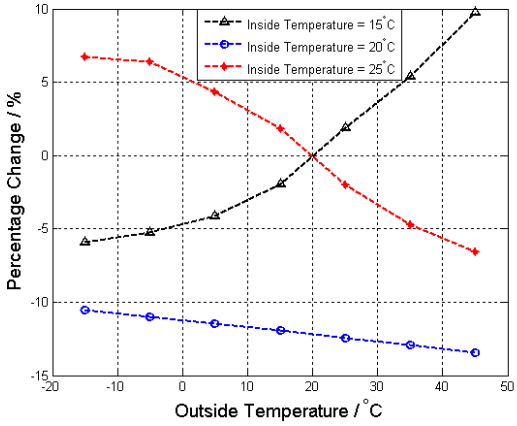

Figure 22. Percentage change in average surface von Mises stress for surface 4.

The results obtained above were for the double pane glass configuration where all the surfaces of the double pane system touching the window frame were considered to be rigid and completely unexpandable. This is not the case in real life as the glass along with the frame is allowed to thermally expand. To simulate such conditions, models were built in COMSOL with the two glass layers free to expand. The complete results for this group of simulations in tabulated form for both the EC and non EC cases are listed in tabulated form in Appendix B.

Also, the results above are for when the temperatures and stresses reach steady state. Time dependent studies for three of the outdoor temperatures at -15˚C, 15˚C and 45˚C were simulated for an indoor temperature of 25˚C. The time dependent study was carried out for completely fixed double pane glass structures with and without the EC layer from a time starting at 0 seconds and ending at 1 hour at intervals of 400 seconds. The complete results for these simulations are tabulated in Appendix C.

Chapter Five: Discussion

The simulations performed for the different configurations of the double pane glass resulted in some very distinct results. Before delving into the meaning of these results, some understanding of the input variables and assumptions need to be made.

The main assumption in all the simulated models is that the intensity of solar radiation is a constant 800W/m^2. The maximum solar radiation intensity on the Earth's surface is around 1000W/m^2 on a horizontal surface with the sun directly above the surface with clear cloud conditions. However, this maximum intensity is not constant everywhere and an average solar radiation intensity for the entire Earth's surface is about 342W/m^2. With reference to [**7**], 800W/m^2 was arbitrarily chosen as the intensity of solar radiation assuming this solar radiation intensity to be higher than the average value but lower than the maximum possible value. This value is a worst case scenario for solar radiation intensity because all the models simulated in this research work assume that this intensity remains constant for as long as it takes for the variables to become steady. In real life, the intensity of solar radiation starts from zero, reaches a peak mid day and then decreases as the day reaches its end. Also, the solar radiation is set to an angle perpendicular to the glass surface for all times, which is usually not true in real life because the solar radiation angles change throughout the day and windows are usually not at right angles to the solar radiation. This number however does cause structural

failure of glass and the effects of the EC layer can be better seen at this value of solar intensity, as will be discussed later in this chapter.

For the structural failure of glass to occur, the maximum von Mises stress induced on the glass has to exceed the ultimate tensile yield stress of glass. The value of ultimate yield stress of glass is anywhere between 33MPa to 70MPa depending of the type of glass and the ambient conditions. The von Mises stress induced on all the different models are compared to this number as a reference point for the structural integrity of the systems simulated. The maximum values of the stresses and not the average values are used for this purpose because even though the average stresses are a lot less than the maximum stresses, the occurrence of a maximum stress higher than the yield stress will cause failure of the glass. The von Mises stresses of surfaces 2 and 3 are not mentioned in this thesis because the stress values for these surfaces were found to have values in between the values for surfaces 1 and 4.

The final assumption of this research is that the temperatures for surface 2 and surface 3 of the double pane glass system are not considered relevant. The reason for this is that these two surfaces aren't interacting with the outdoor or indoor environments although they do contribute to the temperatures of the other two surfaces.

The results of the different studies performed for this research are presented under the following sub chapter headings. All the studies performed are based on the assumptions made above. Comparisons of the results obtained with related works found in the literature are included in the final section of this chapter.

5.1 Completely rigid glass structure

The tables presented in chapter 4 and appendix A along with the figures in chapter 4 are the results for the case where all the surfaces of the double pane window system, both with and without and EC layer, are rigid and do not allow for any thermal expansion. The 3D figures in chapter 4 are representative of the stress and temperature profiles for all the models simulated for all possible cases although the values are different for each case.

For the figures in chapter 4, the outdoor temperature is 45˚C and the indoor temperature is 25˚C. As can be seen in figures 10 and 12, the temperatures between the top surface and the bottom surface have a considerable difference. The reason for this is that the air in between the two glass layers acts as an insulating medium. The aluminum spacer has temperatures similar to the top surface for the case in those figures because aluminum is a very good conductor of heat. The outer surfaces of both glass layers are at similar temperatures to the aluminum spacer because of this property of aluminum. The insulating property of air however causes the top and bottom surfaces to be so different from one another.

These figures also show that the parts of the two glass surfaces in contact with the thin layer of aluminum spacer have temperatures similar to that of the aluminum spacer while the parts of the two glass surfaces not in contact with the aluminum have much different temperatures than the aluminum. There is a high temperature gradient in these two regions of glass because aluminum has a higher thermal conductivity as compared to

glass and although aluminum transfers heat to the glass, the glass cannot transfer the heat as well as the aluminum.

This high temperature gradient contributes to the concentration of high von Mises stresses at the edges of the glass surfaces as seen in figures 11 and 13. The edges have high stress values also because all the edges are not allowed to thermally expand while the glass in the middle can expand in other directions other than the edges. However, figure 11 is different from figure 13 in that the presence of the EC layer causes most of the high stresses to be concentrated near the EC layer while there is significantly less stress around near the bottom glass layer. The reason for this might be that the coefficient of thermal expansion of the EC material is a lot higher than that of both glass and aluminum and so, there is a lot more stress around the regions near the EC layer.

The figures discussed above generalize the temperature and stress profiles of the double pane glass system for all the indoor and outdoor temperature configurations simulated in terms of the distribution and concentration of temperature and stress in the glass system. The tables presented in chapter 4 and appendix A however, compare the effects of those temperature configurations on the maximum and average values of the dependent variables. Figures 15 to 22 summarize the results in those tables.

Figures 15, 16, 19 and 20 show that the addition of the EC layer creates an insulating effect on the two glass layers. At very low outdoor temperatures the maximum and average surface temperatures of both the top and bottom surfaces are increased while at very high outdoor temperatures, these surface temperatures are decreased. This effect is very prominent on the top surface while the temperature change in percentage on the

bottom surface is not as high as compared to the top surface. Also, this insulating effect of the EC layer is most prominent at the extreme outdoor temperature values, both very low and very high. This is the trend for all indoor temperature configurations.

Figures 17 and 18 show that the maximum von Mises stresses for both surface 1 and surface 4 are reduced due to the addition of the EC layer. They also show that for the same indoor and outdoor temperatures, the maximum stresses are reduced the most for surface 1. For indoor temperatures of 20˚C, the decrease in stresses for both surfaces is more consistent for all outdoor temperatures. Similar to the percentage temperature changes of for surfaces 1 and 4, the decrease in maximum von Mises stresses is a lot higher on surface 1 than on surface 4. Surface 1 has a decrease in stress as low as 77% while surface 4 has a lowest percentage decrease in stress of about 14%. Figure 21 shows that the average von Mises stresses for surface 1 decrease for all outdoor temperature configurations while figure 22 shows that this average value does not decrease for all temperature configurations. These figures show that the 20˚C outdoor temperature configuration has 0% average stress change and is like a symmetry point for the stress change plots.

The tables in appendix A give a better picture of the actual temperature and stress values experienced by the two surfaces. The table comparing the maximum surface temperature and stress values suggest that the addition of the EC layer makes the stresses higher on surface 4 as compared to surface 1. However, the maximum stress values are lowered for both surfaces when compared to their corresponding values with the absence of the EC layer. The low thermal conductivity of the EC layer prevents much of the heat

transfer between the aluminum spacer and the upper glass layer but there is no such insulating layer between the bottom glass layer and the aluminum spacer. This is why there isn't as high a thermal gradient on the top surface as compared to the bottom surface and hence, the stresses are lower on the top surface than the bottom surface. The situation is reversed in the absence of the EC layer because although the aluminum spacer is in contact with both glass layers, the air in between the two glass layers insulates much of the heat and thus, the temperature gradient caused by the solar radiation.

This table also gives an insight on the failure conditions of the glass layers. Without the EC layer, almost all maximum stress values for surfaces 1 and 4 exceed 33MPa and some even exceed 70MPa. With the EC layer however, about half of the maximum stresses for the bottom surface are lowered below 33MPa and the top surface stresses never exceed this value. This data shows that at conditions where the glass is likely to fail without the EC layer, the addition of the EC layer significantly reduces the probability of glass failure. Although the average von Mises stress values are not of significant importance, it is notable that no average stress values exceed or even get close to the 33MPa limit. This further illustrates the fact that high stresses are concentrated on the edges while the majority of the surfaces don't experience that high stress values.

5.2 Time dependent study of completely rigid glass structure

The tables in appendix C are obtained by running time dependent simulations of the rigid double pane glass model for an indoor temperature of 25˚C and outdoor temperatures of -15˚C, 15˚C and 45˚C for a period of 1 hour at intervals of 400 seconds.

These simulations were carried out to investigate how long it would take for the temperature and stress values to reach steady state.

From the average and maximum value tables, it is clear that the dependent variables of temperature and von Mises stresses reach near steady state values at around the one hour mark. The progression towards the steady state values is exponential and most of this progression is reached within the first 400 seconds of the simulations. Comparing with the tables in appendix A, it is evident that the average and maximum values are reached within 99% of their corresponding steady state values within an hour and so, it can be concluded that the steady state values take just over an hour to be reached. The trend of temperature and stresses for the top and bottom surfaces for the three temperature configurations are exactly the same as described in the previous section and the insulating properties of the EC layer are clearly seen in these tables as well.

5.3 Free glass structure

Appendix B includes the steady state maximum and average values of temperatures and stresses for the double pane glass structures similar to the ones discussed in previous sections. The differentiating quality of the simulations in this configuration is that the top and bottom glass layers are free to thermally expand. In real life, even though the glass is fixed to a frame, the heat coming from the solar radiation causes thermal expansion of the frame as well as the glass layers. This allows for some expansion to occur in the glass surfaces in contact with the frame which reduces the overall stresses experienced by the glass.

The tables for maximum and average surface temperatures for this configuration are exactly the same as for the rigid glass models. The thermal insulating effect caused by the inclusion of the EC layer is also present in the simulations for this configuration. As the heat transfer calculations are done separate from the solid mechanics calculations in COMSOL, it is not surprising that the results are identical to the rigid glass models discussed in previous sections.

The tables for the von Mises stresses offer more insight on the effect the freedom to expand for the glass layers has on the stress profiles on the two glass surfaces. Most notably, as compared to the rigid models, the top surface maximum stresses are always increased for all temperature configurations when the EC layer is added to the glass structure. For this surface when there is no EC layer, these stress values are always decreased which is the case for the bottom surface both with and without the EC layer. The increase in the maximum von Mises stresses on the top surface causes 9 cases to exceed the 33MPa yield stress. For all configurations however, the maximum stresses on all surface remain below 70MPa.

However, the average von Mises stress value tables follow a different trend. For both surfaces with and without the EC layer, the average stresses are always decreased as compared to the rigid models, although this decrease for all cases is always below 0.2%. This suggests that when the glass layers are free, the average von Mises stresses are always decreased for both surfaces even though the maximum stresses increase for the top surface with the EC layer.

5.4 Comparison of results with other works

Although computer simulations for the temperature profile with and without EC layers for double pane glass have been done in the literature surveyed, there is only one such case where the structural stresses have also been also been simulated by Fischer *et al*. However, their simulations are for an EC layer in between two panes of glass without any air in between them. Also, the heat source used increases from 0 to 800W/m^2 and back to 0 within 20 minutes [**7**]. Simulations done to compare their results using such a ramping up heat source was also done and the temperatures and stresses obtained in COMSOL were very similar to the ones achieved by Fischer *et al*. Although the purpose of this thesis is to study the steady state temperature and stress profiles with a constant radiation source the simulations in COMSOL for the configurations specified in their paper acts as a proof of concept for the models simulated for this thesis.

Similarly, the paper by Piccolo explains a finite difference method simulation of temperature values for a double pane window system with an EC layer. The EC layer is placed on surface 1 however and the ambient temperature values are obtained from actual temperatures in test facilities in Italy. Nonetheless, the time dependent temperature profiles for the actual experiment and simulated values both for with the EC layer and without the EC layer are very similar to the results obtained in this thesis research work. The temperature differences obtained in that paper are not in the order of several degrees and are mostly within one degree, which is similar to this thesis's results. The ambient temperature range used for that paper however does not go below 15˚C.

Chapter Six: Conclusions and Future Work

COMSOL Multiphysics was used to test the temperature and stress characteristics of a specific type of double pane glass with an EC layer for different conditions for the purposes of this research project. Although thermal modeling has been done in recent works for glass containing an EC layer, the subject of thermal stress has not been widely studied. The purpose of this thesis was to study this aspect of the EC layer glass structure along with the temperature characteristics for ambient temperatures varying from -15˚C to 45˚C.

Three different studies were done in COMSOL for the double pane glass with an EC layer on surface 2. The first was the steady state study of a rigid glass structure without the ability to thermally expand. The results for this configuration suggest that for all the ambient temperature conditions, the EC layer acts like insulation from the external temperatures for both the outer and inner surfaces of glass. This is the case for the other two study configurations as well. In this rigid glass structure, both surfaces of glass had their stresses reduced, with the outer surface having higher reduction. This caused the bottom surface to have higher stresses than the top surface. The second was a time dependent study of the same rigid structure. This study verified that the temperature and stress values reach steady state at around the one hour mark after the application of the constant radiation source.

The third study involved the evaluation of the steady state temperature and stress values for the same glass structure when the glass was free to thermally expand. Although the average stresses for all the surfaces always decreased in the presence of the EC layer, the top surface always had an increase in the maximum stresses. For all the studies done, the maximum stresses always occurred at the edges of the glass surfaces.

The cases investigated in this thesis had a constant radiation source being illuminated on the top glass surface. The value of this radiation was chosen so as to investigate the structural failure conditions of the double pane glass structure, although realistically, this value is relatively high. For most of the cases studied, the EC layer prevented the glass surfaces from exceeding the ultimate yield stress of glass by reducing the maximum stress induced on them.

In conclusion, this research was successful in verifying the advantage of the use of an EC material in improving both the thermal and structural performance of a double pane glass structure.

Future work would include the study of the effects of positioning the EC layer on different surfaces or changing some of the input parameters like the convective heat coefficients or the characteristics of the input radiation. The manuscript for a journal article that includes the results of this thesis is under completion by the author in collaboration with Dave Alie from NREL. Another paper studying the effects of surface radiation of the EC layer on the temperature and stress profiles is concurrently under preparation.

References

[1] Energy Information Administration. (2013, September) The U.S. Energy Information Administration (EIA) website. [Online]. http://www.eia.gov/energyexplained/index.cfm?page=us_energy_use

[2] Kavish Prakash Munshi, "Analysis of Life Cycle Costs and Energy Savings of Electrochromic Glazing for an Office Building," Arizona State University, Phoenix, AZ, Master's Thesis 2012.

[3] Ivan P. Parkin and Troy D. Manning, "Intelligent Thermochromic Windows," *Journal of Chemical Education*, vol. 83, no. 3, p. 393, March 2006.

[4] G.K. Megla, "Optical Properties and Applications of Photochromic Glass," *Applied Optics*, vol. 5, no. 6, pp. 945 - 960, June 1966.

[5] Carl M. Lampert, "Smart switchable glazing for solar energy and daylight control ," *Solar Energy Materials and Solar Cells*, vol. 52, no. 3 - 4, pp. 207 - 221, April 1998.

[6] R. David Rauh, "Electrochromic windows: an overview," *Electrochimica Acta*, vol. 44, no. 18, pp. 3165-3176, May 1999.

[7] U. Fischer et al., "Heat Transport and Thermal Expansion of Electrochromic Glazing Systems Due to Solar Irradiation," *International Journal of Thermophysics*, vol. 25, no. 4, pp. 1299 - 1307, 2004.

[8] Andreas Jonsson and Arne Arne Roos, "Evaluation of control strategies for different smart window combinations using computer simulations," *Solar Energy*, vol. 84, no. 1, pp. 1 - 9, 2010.

[9] Alexander Kraft and Matthias Rottman, "Properties, performance and current status of the laminated electrochromic glass of Gesimat," *Solar Energy Materials and Solar Cells*, vol. 93, no. 12, pp. 2088 - 2092, 2009.

[10] Carl M. Lampert, "Chromogenic smart materials," *Materials Today*, vol. 7, no. 3, pp. 28 - 35, March 2004.

[11] Karl-Heinz Heckner and Alexander Kraft, "Similarities between electrochromic windows and thin film batteries," *Solid State Ionics*, vol. 152 - 153, no. 0, pp. 899 - 905, December 2002.

[12] Yung-Sen Lin, Yue-Liang Chiang, and Jhen-Yi Lai, "Effects of oxygen addition to the electrochromic properties of WO3 − z thin films sputtered on flexible PET/ITO substrates," *Solid State Ionics*, vol. 180, no. 1, pp. 99 - 105, February 2009.

[13] Paul M. S. Monk, "Charge Movement through Electrochromic Thin-Film Tungsten Trioxide," *Critical Reviews in Solid State and Materials Sciences*, vol. 24, no. 3, pp. 193 - 226, September 1999.

[14] B. Baloukas, J. M. Lamarre, and L. Martinu, "Electrochromic interference filters fabricated from dense and porous tungsten oxide films," *Solar Energy Materials and Solar Cells*, vol. 95, no. 3, pp. 807 - 815, March 2011.

[15] K. von Rottkay, M. Rubin, and S. J. Wen, "Optical indices of electrochromic tungsten oxide," *Thin Solid Films*, vol. 306, no. 1, pp. 10 - 16, August 1997.

[16] Liying Zhang, Shanxin Xiong, Jan Ma, and Xuehong Lu, "A complementary electrochromic device based on polyaniline-tethered polyhedral oligomeric silsesquioxane and tungsten oxide," *Solar Energy Materials and Solar Cells*, vol. 93, no. 5, pp. 625 - 629, May 2009.

[17] S. H. Baeck, K. S. Choi, T. F. Jaramillo, G. D. Stucky, and E.W. McFarland, "Enhancement of Photocatalytic and Electrochromic Properties of Electrochemically Fabricated Mesoporous WO3 Thin Films," *Advanced Materials*, vol. 15, no. 15, pp. 1269 - 1273, August 2003.

[18] Gunnar A. Niklassona and Claes G. Granqvist, "Electrochromics for smart windows: thin films of tungsten oxide and nickel oxide, and devices based on these," *Journal of Materials Chemistry*, vol. 17, no. 2, pp. 127 - 156, 2007.

[19] A. Gutarra, A. Azens, B. Stjerna, and C. G. Granqvist, "Electrochromism of sputtered fluorinated titanium oxide thin films," *Applied Physics Letters*, vol. 64, no. 13, pp. 1604 - 1606, January 1994.

[20] S. Kalwellis-Mohn and E.W. Grabner, "A secondary cell based on thin layers of zeolite-like nickel hexacyanometallates," *Electrochimica Acta*, vol. 34, no. 8, pp. 1265 - 1269, August 1989.

[21] Gunnar A. Niklasson, Lars Berggren, and Anna-Lena Larsson, "Electrochromic tungsten oxide: the role of defects," *Solar Energy Materials and Solar Cells*, vol. 84, no. 1 - 4, pp. 315 - 328, October 2004.

[22] Haidong Zheng et al., "Nanostructured Tungsten Oxide – Properties, Synthesis, and Applications," *Advanced Functional Materials*, vol. 21, no. 12, pp. 2175 - 2196, 2011.

[23] R Lechner and L. K. Thomas, "All solid state electrochromic devices on glass and polymeric foils," *Solar Energy Materials and Solar Cells*, vol. 54, no. 1 - 4, pp. 139 - 146, 1998.

[24] M.Ahsan Habib and David Glueck, "The electrochromic properties of chemically deposited tungsten oxide films," *Solar Energy Materials*, vol. 18, no. 3 - 4, pp. 127 - 141, March 1989.

[25] Toshihiro Yamase, "Photo- and Electrochromism of Polyoxometalates and Related Materials," *Chemical Reviews*, vol. 98, no. 1, pp. 307 - 326, February 1998.

[26] Se-Hee Lee et al., "Electrochromic mechanism in a-WO3−y thin films," *Applied Physics Letters*, vol. 74, no. 2, pp. 242 - 244, 1999.

[27] A. Bessière et al., "Flexible electrochromic reflectance device based on tungsten oxide for infrared emissivity control," *Journal of Applied Physics*, vol. 91, no. 3, pp. 1589 - 1594, 2002.

[28] Lin Liang et al., "High-performance flexible electrochromic device based on facile semiconductor-to-metal transition realized by WO3.2H2O ultrathin nanosheets," *Scientific Reports*, vol. 3, p. 1936, 2013.

[29] Nilgun Ozer and Carl M. Lampert, "Electrochromic characterization of sol–gel deposited coatings," *Solar Energy Materials and Solar Cells*, vol. 54, no. 1 - 4, pp. 147 - 156, July 1998.

[30] Zheng Jiao, Minghong Wu, Zheng Qin, and Hong Xu, "The electrochromic characteristics of sol–gel-prepared NiO thin film ," *Nanotechnology*, vol. 14, no. 4, p. 458, March 2003.

[31] Walter Estrada, Anne M. Andersson, and Claes G. Granqvist, "Electrochromic nickel-oxide-based coatings made by reactive dc magnetron sputtering: Preparation and optical properties," *Journal of Applied Physics*, vol. 64, no. 7, pp. 3678 - 3683, June 1988.

[32] F Michalak, K von Rottkay, T Richardson, J Slack, and M Rubin, "Electrochromic lithium nickel oxide thin films by RF-sputtering from a LiNiO2 target," *Electrochimica Acta*, vol. 44, no. 18, pp. 3085 - 3092, May 1999.

[33] J. Stefan E. M. Svensson and Claes G. Granqvist, "Optical properties of electrochromic hydrated nickel oxide coatings made by rf sputtering," *Applied Optics*, vol. 26, no. 8, pp. 1554 - 1556, April 1987.

[34] K. Muthu Karuppasamy and A. Subrahmanyam, "The electrochromic and photocatalytic properties of electron beam evaporated vanadium-doped tungsten oxide thin films," *Solar Energy Materials and Solar Cells*, vol. 92, no. 11, pp. 1322 - 1326, November 2008.

[35] M.C.A Fantini, F.F Ferreira, and A Gorenstein, "Theoretical and experimental results on Au–NiO and Au–CoO electrochromic composite films," *Solid State Ionics*, vol. 152 - 153, no. 0, pp. 867 - 872, December 2002.

[36] Roger J. Mortimer, Aubrey L. Dyer, and John R. Reynolds, "Electrochromic organic and polymeric materials for display applications," *Displays*, vol. 27, no. 1, pp. 2 - 18, 2006.

[37] Guanggang Gao et al., "Electrochromic Multilayer Films of Tunable Color by Combination of Copper or Iron Complex and Monolacunary Dawson-Type Polyoxometalate," *The Journal of Physical Chemistry B*, vol. 109, no. 18, pp. 8948 - 8953, June 2005.

[38] Shawn A. Sapp, Gregory A. Sotzing, and John R. Reynolds, "High Contrast Ratio and Fast-Switching Dual Polymer Electrochromic Devices," *Chemistry of Materials*, vol. 10, no. 8, pp. 2101 - 2108, August 1998.

[39] AbuBakr S. Bahaj, Patrick A. B. James, and Mark F. Jentsch, "Potential of emerging glazing technologies for highly glazed buildings in hot arid climates," *Energy and Buildings*, vol. 40, no. 5, pp. 720 - 731, 2008.

[40] A. Piccollo, "Thermal performance of an electrochromic smart window tested in an environmental test cell," *Energy and Buildings*, vol. 42, no. 9, pp. 1409 - 1417, 2010.

[41] David V. Hutton, *Fundamentals of Finite Element Analysis*, 1st ed. New York, United States of America: Mcgraw-Hill, 2004.

[42] Zuomin Dong. (2013, November) University of Victoria Mechanical Engineering Department Website. [Online]. http://www.engr.uvic.ca/~mech410/lectures/FEA_Theory.pdf

[43] COMSOL Multiphysics. (2012, November) COMSOL Multiphysics User's Guide.

[44] COMSOL. (2013, November) Heat Transfer Module User's Guide.

[45] COMSOL. (2012, May) Structural Mechanics Module User's Guide.

[46] Solaglas Ltd. (2011, September) Window Energy Ratings data for double glazed unit specifications from Solaglas Ltd. Specification Sheet.

Appendix A

Difference in maximum surface temperatures due to presence of EC layer

		Without EC		With EC		Difference		% Difference	
T_o/˚C	T_i/˚C	T1/˚C	T4/˚C	T1/˚C	T4/˚C	T1/˚C	T4/˚C	T1/%	T4/%
-15	15	-4.176	12.449	-3.120	12.865	1.056	0.416	25.296	3.340
-15	20	-2.420	17.003	-1.429	17.417	0.991	0.413	40.962	2.430
-15	25	-0.664	21.552	0.263	21.963	0.928	0.411	139.667	1.905
-5	15	2.232	13.274	3.033	13.592	0.801	0.318	35.903	2.395
-5	20	3.987	17.828	4.720	18.143	0.733	0.315	18.377	1.766
-5	25	5.741	22.376	6.407	22.688	0.666	0.312	11.593	1.394
5	15	8.640	14.124	9.167	14.328	0.527	0.204	6.099	1.447
5	20	10.393	18.678	10.848	18.879	0.455	0.201	4.375	1.077
5	25	12.146	23.225	12.530	23.423	0.384	0.198	3.162	0.852
15	15	15.047	15.049	15.682	15.306	0.635	0.257	4.223	1.708
15	20	16.798	19.553	16.955	19.624	0.157	0.071	0.932	0.364
15	25	18.550	24.100	18.632	24.168	0.082	0.068	0.444	0.281
25	15	24.558	20.643	23.998	20.472	-0.560	-0.171	-2.282	-0.829
25	20	24.777	22.796	24.155	22.580	-0.622	-0.216	-2.511	-0.948
25	25	25.000	25.000	24.717	24.921	-0.283	-0.079	-1.134	-0.317
35	15	34.103	26.235	32.244	25.619	-1.859	-0.616	-5.452	-2.348
35	20	34.323	28.386	32.398	27.721	-1.925	-0.665	-5.609	-2.343
35	25	34.545	30.537	32.553	29.822	-1.992	-0.715	-5.766	-2.342
45	15	43.636	31.824	40.398	30.741	-3.238	-1.083	-7.420	-3.404
45	20	43.857	33.974	40.549	32.837	-3.308	-1.137	-7.542	-3.346
45	25	44.080	36.123	40.701	34.932	-3.379	-1.191	-7.665	-3.297

Difference in maximum surface von Mises Stresses due to presence of EC layer

		Without EC		With EC		Difference		% Difference	
T_o/˚C	T_i/˚C	S1/Nm^{-2}	S4/Nm^{-2}	S1/Nm^{-2}	S4/Nm^{-2}	S1/Nm^{-2}	S4/Nm^{-2}	S1/%	S4/%
-15	15	1.01E+08	9.35E+07	2.70E+07	8.34E+07	-7.38E+07	-1.00E+07	-73.23	-10.73
-15	20	9.29E+07	8.44E+07	2.60E+07	7.49E+07	-6.69E+07	-9.53E+06	-71.99	-11.28
-15	25	8.50E+07	7.54E+07	2.51E+07	6.64E+07	-5.99E+07	-9.02E+06	-70.50	-11.96
-5	15	7.42E+07	6.93E+07	1.95E+07	6.19E+07	-5.47E+07	-7.43E+06	-73.77	-10.72
-5	20	6.63E+07	6.03E+07	1.85E+07	5.34E+07	-4.78E+07	-6.92E+06	-72.10	-11.47
-5	25	5.85E+07	5.13E+07	1.76E+07	4.49E+07	-4.09E+07	-6.39E+06	-69.95	-12.46
5	15	4.76E+07	4.52E+07	1.20E+07	4.05E+07	-3.56E+07	-4.75E+06	-74.78	-10.50
5	20	3.98E+07	3.62E+07	1.11E+07	3.20E+07	-2.87E+07	-4.22E+06	-72.21	-11.66
5	25	3.20E+07	2.72E+07	1.01E+07	2.35E+07	-2.18E+07	-3.68E+06	-68.27	-13.51
15	15	2.11E+07	2.11E+07	4.88E+06	1.91E+07	-1.62E+07	-1.97E+06	-76.87	-9.35
15	20	1.33E+07	1.21E+07	3.67E+06	1.06E+07	-9.59E+06	-1.43E+06	-72.33	-11.85
15	25	5.60E+06	3.53E+06	2.86E+06	3.42E+06	-2.74E+06	-1.10E+05	-48.97	-3.11
25	15	5.60E+06	3.53E+06	2.84E+06	3.42E+06	-2.76E+06	-1.09E+05	-49.24	-3.09
25	20	1.33E+07	1.21E+07	3.65E+06	1.06E+07	-9.60E+06	-1.45E+06	-72.44	-12.04
25	25	2.11E+07	2.11E+07	4.87E+06	1.91E+07	-1.62E+07	-2.02E+06	-76.93	-9.56
35	15	3.20E+07	2.72E+07	1.00E+07	2.34E+07	-2.19E+07	-3.84E+06	-68.68	-14.11
35	20	3.98E+07	3.62E+07	1.09E+07	3.18E+07	-2.89E+07	-4.43E+06	-72.56	-12.24
35	25	4.76E+07	4.52E+07	1.19E+07	4.02E+07	-3.57E+07	-5.01E+06	-75.07	-11.09
45	15	5.85E+07	5.13E+07	1.72E+07	4.44E+07	-4.13E+07	-6.90E+06	-70.58	-13.44
45	20	6.63E+07	6.03E+07	1.81E+07	5.28E+07	-4.81E+07	-7.50E+06	-72.67	-12.44
45	25	7.41E+07	6.93E+07	1.90E+07	6.12E+07	-5.50E+07	-8.10E+06	-74.29	-11.69

Difference in average surface temperatures due to presence of EC layer

		Without EC		With EC		Difference		% Difference	
T_o/˚C	T_i/˚C	T1/˚C	T4/˚C	T1/˚C	T4/˚C	T1/˚C	T4/˚C	T1/%	T4/%
-15	15	-12.872	11.079	-9.060	11.583	3.812	0.504	29.611	4.549
-15	20	-12.512	15.402	-8.736	15.901	3.776	0.498	30.178	3.236
-15	25	-12.149	19.721	-8.409	20.213	3.739	0.493	30.781	2.499
-5	15	-3.567	12.365	-0.738	12.747	2.830	0.382	79.321	3.090
-5	20	-3.207	16.688	-0.416	17.064	2.791	0.376	87.035	2.253
-5	25	-2.844	21.006	-0.092	21.375	2.752	0.370	96.775	1.760
5	15	5.724	13.674	7.498	13.918	1.773	0.245	30.978	1.789
5	20	6.085	17.996	7.817	18.234	1.732	0.238	28.461	1.322
5	25	6.448	22.313	8.138	22.544	1.690	0.231	26.207	1.035
15	15	15.004	15.005	15.645	15.096	0.641	0.091	4.271	0.606
15	20	15.365	19.327	15.961	19.410	0.597	0.083	3.883	0.432
15	25	15.728	23.643	16.280	23.719	0.552	0.076	3.507	0.321
25	15	24.271	16.358	23.703	16.278	-0.569	-0.080	-2.343	-0.487
25	20	24.632	20.679	24.016	20.591	-0.616	-0.088	-2.501	-0.424
25	25	24.996	24.995	24.332	24.899	-0.664	-0.096	-2.656	-0.385
35	15	33.526	17.732	31.670	17.465	-1.856	-0.268	-5.536	-1.509
35	20	33.888	22.053	31.981	21.776	-1.906	-0.277	-5.626	-1.254
35	25	34.252	26.368	32.294	26.083	-1.957	-0.286	-5.715	-1.083
45	15	42.770	19.128	39.548	18.654	-3.222	-0.474	-7.534	-2.476
45	20	43.131	23.448	39.856	22.964	-3.276	-0.483	-7.594	-2.061
45	25	43.495	27.762	40.166	27.269	-3.330	-0.493	-7.655	-1.776

Difference in average surface von Mises Stresses due to presence of EC layer

		Without EC		With EC		Difference		% Difference	
T_o/˚C	T_i/˚C	S1/Nm^{-2}	S4/Nm^{-2}	S1/Nm^{-2}	S4/Nm^{-2}	S1/Nm^{-2}	S4/Nm^{-2}	S1/%	S4/%
-15	15	2.47E+07	6.97E+06	2.17E+07	6.56E+06	-3.08E+06	-4.11E+05	-12.43	-5.90
-15	20	2.45E+07	3.83E+06	2.14E+07	3.43E+06	-3.03E+06	-4.04E+05	-12.40	-10.54
-15	25	2.42E+07	1.77E+06	2.12E+07	1.89E+06	-2.99E+06	1.19E+05	-12.37	6.73
-5	15	1.77E+07	5.91E+06	1.55E+07	5.60E+06	-2.28E+06	-3.11E+05	-12.85	-5.26
-5	20	1.75E+07	2.76E+06	1.52E+07	2.45E+06	-2.24E+06	-3.03E+05	-12.81	-11.00
-5	25	1.72E+07	1.95E+06	1.50E+07	2.08E+06	-2.19E+06	1.25E+05	-12.76	6.40
5	15	1.08E+07	4.84E+06	9.32E+06	4.64E+06	-1.43E+06	-1.98E+05	-13.31	-4.09
5	20	1.05E+07	1.67E+06	9.09E+06	1.47E+06	-1.39E+06	-1.91E+05	-13.23	-11.47
5	25	1.02E+07	2.27E+06	8.86E+06	2.37E+06	-1.34E+06	9.84E+04	-13.14	4.34
15	15	3.77E+06	3.77E+06	3.25E+06	3.70E+06	-5.24E+05	-7.28E+04	-13.90	-1.93
15	20	3.49E+06	5.59E+05	3.01E+06	4.92E+05	-4.76E+05	-6.68E+04	-13.65	-11.95
15	25	3.22E+06	2.79E+06	2.79E+06	2.84E+06	-4.29E+05	5.08E+04	-13.32	1.82
25	15	3.22E+06	2.79E+06	2.78E+06	2.84E+06	-4.41E+05	5.36E+04	-13.72	1.92
25	20	3.49E+06	5.63E+05	3.00E+06	4.93E+05	-4.91E+05	-7.00E+04	-14.07	-12.44
25	25	3.77E+06	3.77E+06	3.23E+06	3.69E+06	-5.41E+05	-7.68E+04	-14.35	-2.04
35	15	1.02E+07	2.24E+06	8.71E+06	2.36E+06	-1.46E+06	1.21E+05	-14.39	5.41
35	20	1.05E+07	1.70E+06	8.94E+06	1.48E+06	-1.52E+06	-2.20E+05	-14.50	-12.93
35	25	1.07E+07	4.87E+06	9.17E+06	4.64E+06	-1.57E+06	-2.29E+05	-14.61	-4.71
45	15	1.71E+07	1.86E+06	1.46E+07	2.04E+06	-2.55E+06	1.81E+05	-14.86	9.74
45	20	1.74E+07	2.85E+06	1.48E+07	2.47E+06	-2.60E+06	-3.83E+05	-14.93	-13.43
45	25	1.77E+07	6.00E+06	1.50E+07	5.61E+06	-2.65E+06	-3.95E+05	-15.01	-6.58

Appendix B

Difference in maximum surface temperatures due to presence of EC layer when the glass layers are free to move

		Without EC		With EC		Difference		% Difference	
T_o/˚C	T_i/˚C	T1/˚C	T4/˚C	T1/˚C	T4/˚C	T1/˚C	T4/˚C	T1/%	T4/%
-15	15	-4.176	12.449	-3.120	12.865	1.056	0.416	25.296	3.340
-15	20	-2.420	17.003	-1.429	17.417	0.991	0.413	40.962	2.430
-15	25	-0.664	21.552	0.263	21.963	0.928	0.411	139.667	1.905
-5	15	2.232	13.274	3.033	13.592	0.801	0.318	35.903	2.395
-5	20	3.987	17.828	4.720	18.143	0.733	0.315	18.377	1.766
-5	25	5.741	22.376	6.407	22.688	0.666	0.312	11.593	1.394
5	15	8.640	14.124	9.167	14.328	0.527	0.204	6.099	1.447
5	20	10.393	18.678	10.848	18.879	0.455	0.201	4.375	1.077
5	25	12.146	23.225	12.530	23.423	0.384	0.198	3.162	0.852
15	15	15.047	15.049	15.682	15.306	0.635	0.257	4.223	1.708
15	20	16.798	19.553	16.955	19.624	0.157	0.071	0.932	0.364
15	25	18.550	24.100	18.632	24.168	0.082	0.068	0.444	0.281
25	15	24.558	20.643	23.998	20.472	-0.560	-0.171	-2.282	-0.829
25	20	24.777	22.796	24.155	22.580	-0.622	-0.216	-2.511	-0.948
25	25	25.000	25.000	24.717	24.921	-0.283	-0.079	-1.134	-0.317
35	15	34.103	26.235	32.244	25.619	-1.859	-0.616	-5.452	-2.348
35	20	34.323	28.386	32.398	27.721	-1.925	-0.665	-5.609	-2.343
35	25	34.545	30.537	32.553	29.822	-1.992	-0.715	-5.766	-2.342
45	15	43.636	31.824	40.398	30.741	-3.238	-1.083	-7.420	-3.404
45	20	43.857	33.974	40.549	32.837	-3.308	-1.137	-7.542	-3.346
45	25	44.080	36.123	40.701	34.932	-3.379	-1.191	-7.665	-3.297

Difference in maximum surface von Mises Stresses due to presence of EC layer when the glass layers are free to move

		Without EC		With EC		Difference		% Difference	
T_o/˚C	T_i/˚C	S1/Nm^{-2}	S4/Nm^{-2}	S1/Nm^{-2}	S4/Nm^{-2}	S1/Nm^{-2}	S4/Nm^{-2}	S1/%	S4/%
-15	15	3.56E+07	2.90E+07	5.99E+07	2.71E+07	2.43E+07	-1.89E+06	68.04	-6.54
-15	20	3.36E+07	2.59E+07	5.84E+07	2.40E+07	2.48E+07	-1.85E+06	73.66	-7.14
-15	25	3.16E+07	2.28E+07	5.68E+07	2.10E+07	2.52E+07	-1.80E+06	79.82	-7.89
-5	15	2.60E+07	2.16E+07	4.30E+07	2.02E+07	1.70E+07	-1.41E+06	65.21	-6.52
-5	20	2.40E+07	1.85E+07	4.15E+07	1.71E+07	1.75E+07	-1.36E+06	72.90	-7.34
-5	25	2.20E+07	1.54E+07	4.00E+07	1.41E+07	1.80E+07	-1.30E+06	81.65	-8.45
5	15	1.64E+07	1.42E+07	2.63E+07	1.33E+07	9.85E+06	-8.91E+05	59.88	-6.29
5	20	1.44E+07	1.11E+07	2.48E+07	1.02E+07	1.04E+07	-8.35E+05	72.13	-7.54
5	25	1.24E+07	8.07E+06	2.33E+07	7.28E+06	1.08E+07	-7.85E+05	87.31	-9.73
15	15	6.90E+06	6.89E+06	9.73E+06	6.60E+06	2.84E+06	-2.92E+05	41.16	-4.24
15	20	4.80E+06	3.69E+06	8.22E+06	3.41E+06	3.42E+06	-2.86E+05	71.36	-7.74
15	25	3.59E+06	3.15E+06	6.71E+06	3.20E+06	3.11E+06	5.57E+04	86.70	1.77
25	15	3.59E+06	3.15E+06	6.68E+06	3.21E+06	3.09E+06	5.88E+04	85.91	1.87
25	20	4.79E+06	3.70E+06	8.18E+06	3.40E+06	3.38E+06	-2.94E+05	70.58	-7.95
25	25	6.89E+06	6.89E+06	9.69E+06	6.59E+06	2.79E+06	-3.06E+05	40.53	-4.43
35	15	1.24E+07	8.07E+06	2.29E+07	7.24E+06	1.05E+07	-8.38E+05	84.78	-10.38
35	20	1.44E+07	1.11E+07	2.44E+07	1.02E+07	1.00E+07	-9.04E+05	69.80	-8.16
35	25	1.64E+07	1.42E+07	2.59E+07	1.32E+07	9.48E+06	-9.77E+05	57.71	-6.90
45	15	2.20E+07	1.54E+07	3.90E+07	1.40E+07	1.70E+07	-1.47E+06	77.57	-9.52
45	20	2.40E+07	1.85E+07	4.05E+07	1.69E+07	1.65E+07	-1.55E+06	69.01	-8.37
45	25	2.60E+07	2.16E+07	4.20E+07	1.99E+07	1.60E+07	-1.62E+06	61.48	-7.54

Difference in average surface temperatures due to presence of EC layer when the glass layers are free to move

		Without EC		With EC		Difference		% Difference	
T_o/˚C	T_i/˚C	T1/˚C	T4/˚C	T1/˚C	T4/˚C	T1/˚C	T4/˚C	T1/%	T4/%
-15	15	-12.872	11.079	-9.060	11.583	3.812	0.504	29.611	4.549
-15	20	-12.512	15.402	-8.736	15.901	3.776	0.498	30.178	3.236
-15	25	-12.149	19.721	-8.409	20.213	3.739	0.493	30.781	2.499
-5	15	-3.567	12.365	-0.738	12.747	2.830	0.382	79.321	3.090
-5	20	-3.207	16.688	-0.416	17.064	2.791	0.376	87.035	2.253
-5	25	-2.844	21.006	-0.092	21.375	2.752	0.370	96.775	1.760
5	15	5.724	13.674	7.498	13.918	1.773	0.245	30.978	1.789
5	20	6.085	17.996	7.817	18.234	1.732	0.238	28.461	1.322
5	25	6.448	22.313	8.138	22.544	1.690	0.231	26.207	1.035
15	15	15.004	15.005	15.645	15.096	0.641	0.091	4.271	0.606
15	20	15.365	19.327	15.961	19.410	0.597	0.083	3.883	0.432
15	25	15.728	23.643	16.280	23.719	0.552	0.076	3.507	0.321
25	15	24.271	16.358	23.703	16.278	-0.569	-0.080	-2.343	-0.487
25	20	24.632	20.679	24.016	20.591	-0.616	-0.088	-2.501	-0.424
25	25	24.996	24.995	24.332	24.899	-0.664	-0.096	-2.656	-0.385
35	15	33.526	17.732	31.670	17.465	-1.856	-0.268	-5.536	-1.509
35	20	33.888	22.053	31.981	21.776	-1.906	-0.277	-5.626	-1.254
35	25	34.252	26.368	32.294	26.083	-1.957	-0.286	-5.715	-1.083
45	15	42.770	19.128	39.548	18.654	-3.222	-0.474	-7.534	-2.476
45	20	43.131	23.448	39.856	22.964	-3.276	-0.483	-7.594	-2.061
45	25	43.495	27.762	40.166	27.269	-3.330	-0.493	-7.655	-1.776

Difference in average surface von Mises Stresses due to presence of EC layer when the glass layers are free to move

		Without EC		With EC		Difference		% Difference	
T_o/°C	T_i/°C	S1/Nm^{-2}	S4/Nm^{-2}	S1/Nm^{-2}	S4/Nm^{-2}	S1/Nm^{-2}	S4/Nm^{-2}	S1/%	S4/%
-15	15	2.31E+07	6.04E+06	1.70E+07	5.67E+06	-6.11E+06	-3.68E+05	-26.43	-6.10
-15	20	2.29E+07	3.08E+06	1.68E+07	2.72E+06	-6.05E+06	-3.59E+05	-26.43	-11.67
-15	25	2.27E+07	1.62E+06	1.67E+07	1.82E+06	-6.00E+06	2.04E+05	-26.43	12.58
-5	15	1.66E+07	5.19E+06	1.21E+07	4.91E+06	-4.43E+06	-2.79E+05	-26.78	-5.37
-5	20	1.63E+07	2.22E+06	1.20E+07	1.95E+06	-4.38E+06	-2.70E+05	-26.78	-12.18
-5	25	1.61E+07	1.87E+06	1.18E+07	2.04E+06	-4.32E+06	1.76E+05	-26.77	9.41
5	15	1.00E+07	4.33E+06	7.30E+06	4.15E+06	-2.72E+06	-1.77E+05	-27.13	-4.10
5	20	9.80E+06	1.34E+06	7.14E+06	1.17E+06	-2.66E+06	-1.70E+05	-27.13	-12.69
5	25	9.59E+06	2.22E+06	6.99E+06	2.34E+06	-2.60E+06	1.25E+05	-27.11	5.62
15	15	3.48E+06	3.48E+06	2.52E+06	3.41E+06	-9.58E+05	-6.47E+04	-27.52	-1.86
15	20	3.26E+06	4.51E+05	2.37E+06	3.91E+05	-8.97E+05	-5.96E+04	-27.48	-13.21
15	25	3.06E+06	2.71E+06	2.22E+06	2.76E+06	-8.37E+05	4.90E+04	-27.39	1.81
25	15	3.06E+06	2.71E+06	2.21E+06	2.76E+06	-8.48E+05	5.16E+04	-27.72	1.90
25	20	3.26E+06	4.55E+05	2.35E+06	3.92E+05	-9.08E+05	-6.25E+04	-27.84	-13.74
25	25	3.48E+06	3.48E+06	2.51E+06	3.41E+06	-9.71E+05	-6.82E+04	-27.90	-1.96
35	15	9.57E+06	2.18E+06	6.88E+06	2.33E+06	-2.69E+06	1.47E+05	-28.16	6.74
35	20	9.78E+06	1.37E+06	7.02E+06	1.18E+06	-2.76E+06	-1.96E+05	-28.20	-14.28
35	25	1.00E+07	4.36E+06	7.17E+06	4.16E+06	-2.82E+06	-2.05E+05	-28.23	-4.71
45	15	1.61E+07	1.78E+06	1.15E+07	2.01E+06	-4.59E+06	2.33E+05	-28.53	13.13
45	20	1.63E+07	2.31E+06	1.16E+07	1.97E+06	-4.65E+06	-3.42E+05	-28.56	-14.82
45	25	1.65E+07	5.28E+06	1.18E+07	4.92E+06	-4.72E+06	-3.54E+05	-28.59	-6.71

Appendix C

Time dependent study of the difference in maximum surface temperatures due to presence of EC layer

T_o/˚C	Time/s	Without EC		With EC		Difference		% Difference	
		T1/˚C	T4/˚C	T1/˚C	T4/˚C	T1/˚C	T4/˚C	T1/%	T4/%
-15	0	19.98	20.00	19.98	20.00	0.00	0.00	0.00	0.00
-15	400	9.47	22.03	9.00	22.32	-0.48	0.29	-5.05	1.31
-15	800	5.24	21.87	4.57	22.23	-0.67	0.37	-12.83	1.69
-15	1200	2.88	21.75	2.26	22.10	-0.63	0.35	-21.78	1.59
-15	1600	1.34	21.64	1.16	22.00	-0.18	0.36	-13.60	1.67
-15	2000	0.42	21.59	0.77	21.98	0.35	0.39	82.89	1.80
-15	2400	0.01	21.57	0.56	21.97	0.55	0.41	7952.38	1.88
-15	2800	-0.17	21.56	0.44	21.97	0.61	0.41	351.07	1.91
-15	3200	-0.25	21.55	0.37	21.97	0.61	0.41	246.42	1.92
-15	3600	-0.28	21.55	0.32	21.96	0.60	0.41	215.29	1.91
15	0	20.00	20.00	20.00	20.00	0.00	0.00	0.00	0.00
15	400	19.19	22.52	19.00	22.53	-0.20	0.01	-1.04	0.07
15	800	19.06	23.36	18.81	23.38	-0.26	0.02	-1.34	0.10
15	1200	18.98	23.82	18.71	23.81	-0.27	-0.02	-1.42	-0.07
15	1600	18.94	24.02	18.66	24.04	-0.28	0.02	-1.49	0.07
15	2000	18.93	24.09	18.64	24.14	-0.29	0.04	-1.53	0.18
15	2400	18.93	24.11	18.63	24.17	-0.29	0.06	-1.55	0.25
15	2800	18.92	24.11	18.63	24.18	-0.29	0.07	-1.55	0.27
15	3200	18.92	24.11	18.63	24.17	-0.29	0.07	-1.55	0.28
15	3600	18.92	24.10	18.63	24.17	-0.29	0.07	-1.55	0.28
45	0	20.01	20.00	20.01	20.00	0.00	0.00	0.00	0.00
45	400	38.48	26.68	37.12	26.36	-1.36	-0.31	-3.52	-1.17
45	800	42.21	30.87	40.05	30.47	-2.16	-0.40	-5.13	-1.29
45	1200	43.40	33.23	40.62	32.80	-2.78	-0.43	-6.41	-1.29
45	1600	43.91	34.78	40.73	34.01	-3.18	-0.77	-7.25	-2.22
45	2000	44.07	35.71	40.71	34.57	-3.36	-1.14	-7.63	-3.20
45	2400	44.07	36.13	40.70	34.80	-3.37	-1.33	-7.65	-3.68
45	2800	44.08	36.32	40.70	34.89	-3.38	-1.42	-7.67	-3.92
45	3200	44.08	36.40	40.70	34.93	-3.38	-1.47	-7.67	-4.04
45	3600	44.08	36.43	40.70	34.93	-3.38	-1.49	-7.68	-4.10

Time dependent study of the difference in maximum surface von Mises stresses due to presence of EC layer

T_o/˚C	Time/s	Without EC		With EC		Difference		% Difference	
		S1/Nm^{-2}	S4/Nm^{-2}	S1/Nm^{-2}	S4/Nm^{-2}	S1/Nm^{-2}	S4/Nm^{-2}	S1/%	S4/%
-15	0	2.14E+04	1.64E+03	2.14E+04	1.64E+03	-1.73E+00	1.29E-01	-0.01	0.01
-15	400	3.90E+07	3.01E+07	1.86E+07	2.86E+07	-2.05E+07	-1.54E+06	-52.40	-5.09
-15	800	5.92E+07	4.95E+07	2.31E+07	4.77E+07	-3.61E+07	-1.83E+06	-60.95	-3.70
-15	1200	7.01E+07	6.04E+07	2.43E+07	5.76E+07	-4.58E+07	-2.84E+06	-65.31	-4.71
-15	1600	7.72E+07	6.76E+07	2.47E+07	6.24E+07	-5.25E+07	-5.17E+06	-67.97	-7.64
-15	2000	8.15E+07	7.19E+07	2.49E+07	6.42E+07	-5.66E+07	-7.76E+06	-69.48	-10.79
-15	2400	8.34E+07	7.39E+07	2.50E+07	6.51E+07	-5.85E+07	-8.77E+06	-70.08	-11.87
-15	2800	8.42E+07	7.48E+07	2.50E+07	6.57E+07	-5.92E+07	-9.10E+06	-70.32	-12.17
-15	3200	8.46E+07	7.51E+07	2.50E+07	6.60E+07	-5.96E+07	-9.15E+06	-70.41	-12.18
-15	3600	8.47E+07	7.53E+07	2.51E+07	6.62E+07	-5.97E+07	-9.11E+06	-70.43	-12.10
15	0	3.06E+03	1.64E+03	3.06E+03	1.64E+03	-2.20E-01	-1.72E-02	-0.01	0.00
15	400	3.20E+06	1.98E+06	2.29E+06	1.94E+06	-9.04E+05	-4.02E+04	-28.27	-2.03
15	800	4.41E+06	2.80E+06	2.71E+06	2.73E+06	-1.70E+06	-7.52E+04	-38.54	-2.68
15	1200	5.07E+06	3.25E+06	2.83E+06	3.10E+06	-2.24E+06	-1.42E+05	-44.25	-4.36
15	1600	5.37E+06	3.44E+06	2.86E+06	3.31E+06	-2.51E+06	-1.36E+05	-46.69	-3.94
15	2000	5.49E+06	3.51E+06	2.87E+06	3.39E+06	-2.63E+06	-1.23E+05	-47.82	-3.51
15	2400	5.53E+06	3.53E+06	2.86E+06	3.42E+06	-2.67E+06	-1.16E+05	-48.28	-3.27
15	2800	5.54E+06	3.53E+06	2.86E+06	3.42E+06	-2.68E+06	-1.12E+05	-48.43	-3.18
15	3200	5.54E+06	3.53E+06	2.86E+06	3.42E+06	-2.69E+06	-1.11E+05	-48.45	-3.16
15	3600	5.54E+06	3.53E+06	2.86E+06	3.42E+06	-2.68E+06	-1.11E+05	-48.43	-3.15
45	0	1.53E+04	1.64E+03	1.53E+04	1.64E+03	-1.29E+00	-1.65E-01	-0.01	-0.01
45	400	3.30E+07	2.82E+07	1.32E+07	2.59E+07	-1.99E+07	-2.36E+06	-60.18	-8.37
45	800	5.12E+07	4.61E+07	1.67E+07	4.28E+07	-3.45E+07	-3.32E+06	-67.31	-7.21
45	1200	6.13E+07	5.62E+07	1.81E+07	5.25E+07	-4.31E+07	-3.78E+06	-70.43	-6.72
45	1600	6.79E+07	6.29E+07	1.87E+07	5.74E+07	-4.92E+07	-5.51E+06	-72.46	-8.76
45	2000	7.18E+07	6.70E+07	1.89E+07	5.97E+07	-5.29E+07	-7.28E+06	-73.68	-10.87
45	2400	7.37E+07	6.89E+07	1.90E+07	6.07E+07	-5.47E+07	-8.19E+06	-74.21	-11.90
45	2800	7.45E+07	6.97E+07	1.90E+07	6.10E+07	-5.54E+07	-8.65E+06	-74.44	-12.41
45	3200	7.48E+07	7.00E+07	1.90E+07	6.12E+07	-5.58E+07	-8.87E+06	-74.54	-12.66
45	3600	7.49E+07	7.02E+07	1.90E+07	6.12E+07	-5.59E+07	-8.97E+06	-74.59	-12.79

Time dependent study of the difference in average surface temperatures due to presence of EC layer

T_o/˚C	Time/s	Without EC		With EC		Difference		% Difference	
		T1/˚C	T4/˚C	T1/˚C	T4/˚C	T1/˚C	T4/˚C	T1/%	T4/%
-15	0	19.98	20.00	19.98	20.00	0.00	0.00	0.00	0.00
-15	400	-3.96	21.02	-3.44	21.23	0.52	0.20	13.04	0.97
-15	800	-9.43	20.66	-7.93	20.94	1.50	0.28	15.90	1.34
-15	1200	-11.10	20.32	-8.45	20.59	2.65	0.27	23.91	1.35
-15	1600	-11.85	20.05	-8.42	20.38	3.43	0.33	28.94	1.65
-15	2000	-12.12	19.88	-8.39	20.31	3.73	0.43	30.75	2.15
-15	2400	-12.15	19.79	-8.39	20.27	3.76	0.47	30.92	2.38
-15	2800	-12.14	19.76	-8.40	20.24	3.74	0.49	30.82	2.47
-15	3200	-12.13	19.74	-8.40	20.23	3.73	0.49	30.77	2.48
-15	3600	-12.13	19.74	-8.40	20.22	3.73	0.49	30.75	2.47
15	0	20.00	20.00	20.00	20.00	0.00	0.00	0.00	0.00
15	400	16.76	22.24	17.04	22.26	0.28	0.01	1.66	0.06
15	800	16.04	23.02	16.48	23.05	0.44	0.02	2.73	0.10
15	1200	15.77	23.43	16.32	23.42	0.55	-0.01	3.49	-0.04
15	1600	15.71	23.60	16.27	23.62	0.56	0.02	3.56	0.08
15	2000	15.72	23.65	16.27	23.70	0.55	0.04	3.51	0.18
15	2400	15.73	23.67	16.28	23.72	0.54	0.06	3.46	0.23
15	2800	15.74	23.66	16.28	23.73	0.54	0.06	3.44	0.26
15	3200	15.74	23.66	16.28	23.72	0.54	0.06	3.44	0.26
15	3600	15.74	23.66	16.28	23.72	0.54	0.06	3.43	0.26
45	0	20.01	20.00	20.01	20.00	0.00	0.00	0.00	0.00
45	400	37.29	23.60	36.04	23.58	-1.25	-0.02	-3.35	-0.10
45	800	41.35	25.57	39.28	25.56	-2.07	-0.02	-5.00	-0.06
45	1200	42.64	26.60	40.04	26.59	-2.60	-0.01	-6.09	-0.06
45	1600	43.24	27.24	40.20	27.05	-3.04	-0.19	-7.03	-0.69
45	2000	43.47	27.58	40.18	27.22	-3.29	-0.37	-7.56	-1.34
45	2400	43.50	27.72	40.16	27.27	-3.34	-0.45	-7.67	-1.63
45	2800	43.50	27.76	40.16	27.28	-3.34	-0.48	-7.68	-1.75
45	3200	43.50	27.77	40.16	27.27	-3.34	-0.50	-7.67	-1.79
45	3600	43.50	27.77	40.17	27.27	-3.34	-0.50	-7.67	-1.81

Time dependent study of the difference in average surface von Mises stresses due to presence of EC layer

T_o/˚C	Time/s	Without EC		With EC		Difference		% Difference	
		S1/Nm^{-2}	S4/Nm^{-2}	S1/Nm^{-2}	S4/Nm^{-2}	S1/Nm^{-2}	S4/Nm^{-2}	S1/%	S4/%
-15	0	1.56E+04	1.19E+03	1.56E+04	1.19E+03	1.03E-01	4.62E-03	0.00	0.00
-15	400	1.80E+07	1.35E+06	1.75E+07	1.49E+06	-4.80E+05	1.33E+05	-2.67	9.83
-15	800	2.21E+07	1.60E+06	2.09E+07	1.79E+06	-1.27E+06	1.90E+05	-5.72	11.90
-15	1200	2.34E+07	1.67E+06	2.12E+07	1.84E+06	-2.16E+06	1.74E+05	-9.22	10.44
-15	1600	2.40E+07	1.71E+06	2.12E+07	1.86E+06	-2.75E+06	1.51E+05	-11.48	8.83
-15	2000	2.42E+07	1.74E+06	2.12E+07	1.87E+06	-2.98E+06	1.35E+05	-12.32	7.76
-15	2400	2.42E+07	1.75E+06	2.12E+07	1.88E+06	-3.00E+06	1.30E+05	-12.41	7.41
-15	2800	2.42E+07	1.75E+06	2.12E+07	1.88E+06	-2.99E+06	1.27E+05	-12.37	7.26
-15	3200	2.42E+07	1.76E+06	2.12E+07	1.88E+06	-2.99E+06	1.26E+05	-12.35	7.19
-15	3600	2.42E+07	1.76E+06	2.12E+07	1.89E+06	-2.99E+06	1.26E+05	-12.34	7.16
15	0	2.22E+03	1.19E+03	2.22E+03	1.19E+03	6.35E-03	5.75E-03	0.00	0.00
15	400	2.44E+06	1.70E+06	2.22E+06	1.71E+06	-2.18E+05	1.01E+04	-8.93	0.59
15	800	2.98E+06	2.30E+06	2.64E+06	2.32E+06	-3.42E+05	1.70E+04	-11.47	0.74
15	1200	3.18E+06	2.62E+06	2.76E+06	2.61E+06	-4.28E+05	-8.34E+03	-13.45	-0.32
15	1600	3.23E+06	2.75E+06	2.79E+06	2.76E+06	-4.35E+05	1.22E+04	-13.48	0.44
15	2000	3.23E+06	2.79E+06	2.80E+06	2.82E+06	-4.29E+05	3.04E+04	-13.31	1.09
15	2400	3.22E+06	2.80E+06	2.79E+06	2.84E+06	-4.24E+05	4.03E+04	-13.19	1.44
15	2800	3.21E+06	2.80E+06	2.79E+06	2.84E+06	-4.22E+05	4.44E+04	-13.14	1.59
15	3200	3.21E+06	2.80E+06	2.79E+06	2.84E+06	-4.21E+05	4.57E+04	-13.13	1.63
15	3600	3.21E+06	2.80E+06	2.79E+06	2.84E+06	-4.21E+05	4.59E+04	-13.13	1.64
45	0	1.11E+04	1.19E+03	1.11E+04	1.19E+03	8.74E-02	6.45E-03	0.00	0.00
45	400	1.30E+07	2.76E+06	1.20E+07	2.74E+06	-1.02E+06	-2.47E+04	-7.81	-0.90
45	800	1.61E+07	4.29E+06	1.44E+07	4.26E+06	-1.67E+06	-2.24E+04	-10.38	-0.52
45	1200	1.70E+07	5.08E+06	1.50E+07	5.06E+06	-2.08E+06	-2.31E+04	-12.23	-0.45
45	1600	1.75E+07	5.58E+06	1.51E+07	5.42E+06	-2.43E+06	-1.58E+05	-13.88	-2.83
45	2000	1.77E+07	5.86E+06	1.50E+07	5.56E+06	-2.62E+06	-2.98E+05	-14.82	-5.08
45	2400	1.77E+07	5.96E+06	1.50E+07	5.60E+06	-2.66E+06	-3.62E+05	-15.03	-6.08
45	2800	1.77E+07	6.00E+06	1.50E+07	5.61E+06	-2.66E+06	-3.89E+05	-15.04	-6.49
45	3200	1.77E+07	6.01E+06	1.50E+07	5.61E+06	-2.66E+06	-4.00E+05	-15.04	-6.65
45	3600	1.77E+07	6.01E+06	1.50E+07	5.61E+06	-2.66E+06	-4.04E+05	-15.04	-6.72